

# Dark matter Halos

---

- ❖ **Dark matter halos profiles:**
  - ❖ **DM only: NFW vs. Einasto**
  - ❖ **Halo concentration: evolution with time**
  
- ❖ **Dark matter halos profiles: Effects of baryons**
  - ❖ **Adiabatic contraction**
  - ❖ **Cusps and cores in central regions of halos**

$$\rho(r) = \frac{\rho_0 r_s^3}{r(r + r_s)^2}, \quad M(r) = M_{\text{vir}} \times \frac{f(x)}{f(C)},$$

$$f(x) \equiv \ln(1 + x) - \frac{x}{1 + x}, \quad x \equiv \frac{r}{r_s},$$

$$C \equiv \frac{r_{\text{vir}}}{r_s},$$

$$r_{\text{vir}}(M_{\text{vir}}) = 443 h^{-1} \text{ kpc} \left( \frac{M_{\text{vir}} / 10^{11} h^{-1} M_{\odot}}{\Omega_0 \delta_{\text{th}}} \right)^{1/3}$$

$$M_{\text{vir}} \equiv \frac{4\pi}{3} \rho_{\text{cr}} \Omega_0 \delta_{\text{th}} r_{\text{vir}}^3.$$

$$V_{\text{max}}^2 = \frac{GM_{\text{vir}}}{r_s} \times \frac{f(2)}{2f(C)}, \quad f(2) \approx 0.432,$$

$$M(r) = \frac{r_s V_{\text{max}}^2}{G} \times \frac{2f(x)}{f(2)}, \quad \Omega^2(r) = \frac{V_{\text{max}}^2}{r_s^2} \times \frac{2f(x)}{x^3 f(2)},$$

$$V_{\text{esc}}^2 = -2\phi(r) = 4V_{\text{max}}^2 \times \frac{\ln(1 + x)}{xf(2)},$$

## NFW:

$$\Omega^2(r) = \frac{GM}{r^3} = \frac{GM_{\text{vir}}}{r_s^3 f(C)} \times \frac{f(x)}{x^3},$$

$$\phi(r) = -\frac{GM_{\text{vir}}}{r_s f(C)} \times \frac{f(x) + x/(1 + x)}{x}$$

## Einasto:

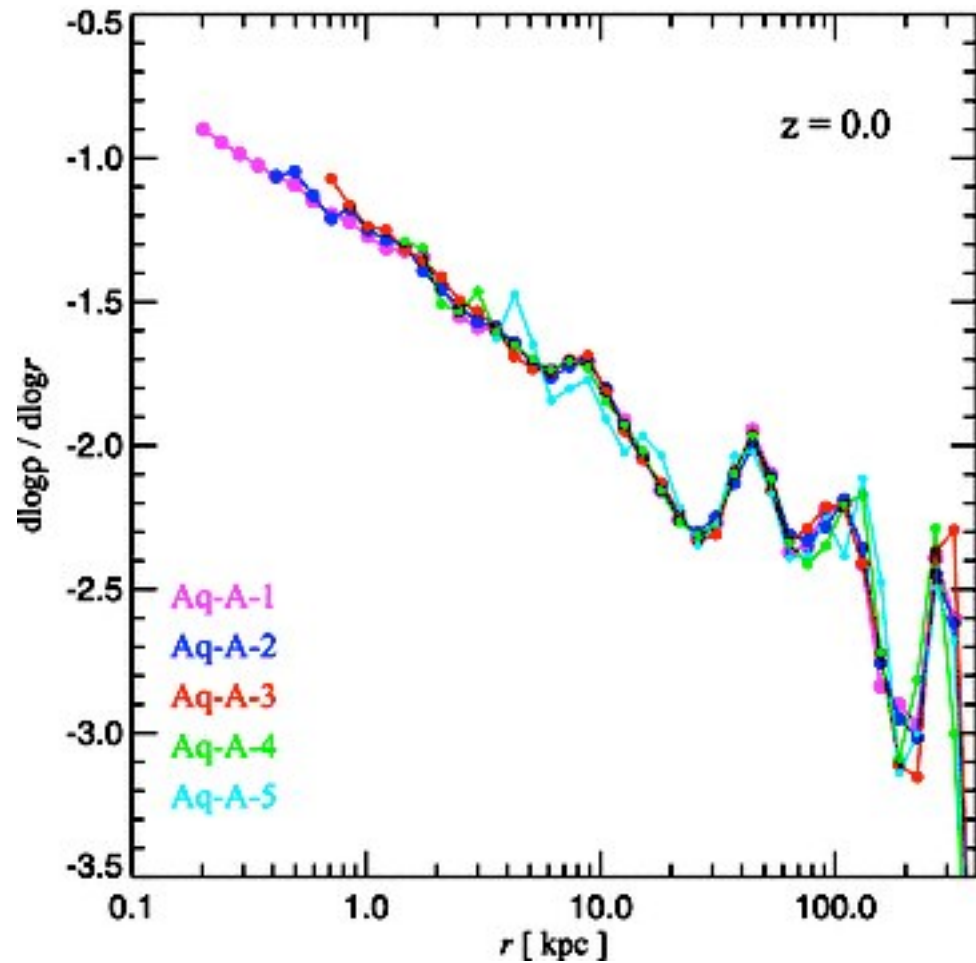
$$\rho_{\text{Ein}}(r) = \rho_0 \exp\left(-\frac{2}{\alpha} [x^\alpha - 1]\right), \quad x \equiv \frac{r}{r_{-2}}$$

the radius  $r_{-2}$  is the characteristic radius of the halo where the logarithmic slope of the density profile  $d \log(\rho)/d \log(R)$  is equal to -2.

$$f_E(x, \alpha) = e^{\frac{2}{\alpha}} \int_0^x x^2 e^{-\frac{2}{\alpha} x^\alpha} dx,$$

$$x \equiv \frac{r}{r_{-2}}, \quad C = \frac{R_{\text{vir}}}{r_{-2}}.$$

# Dark matter profiles: central profile

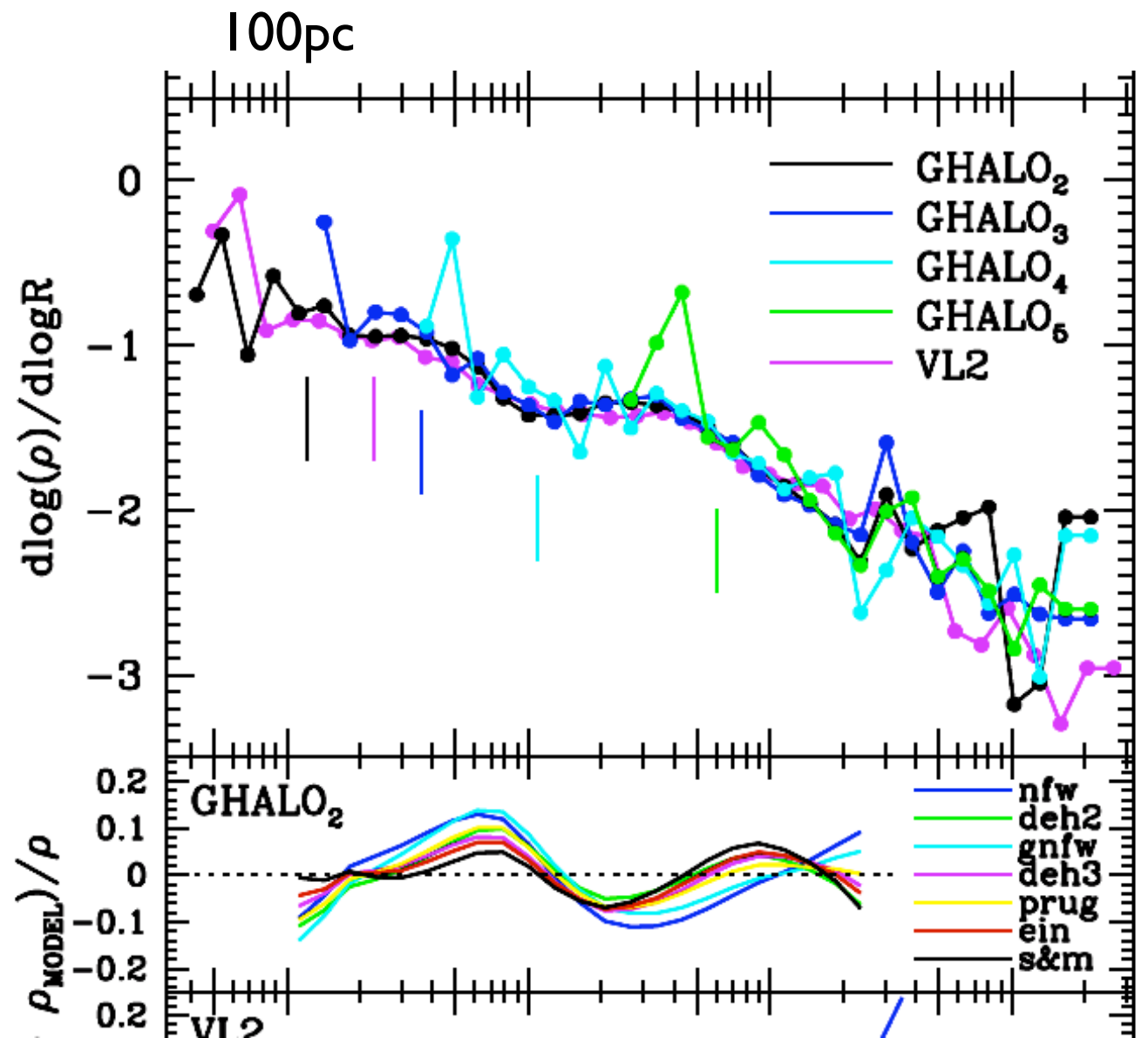


Aquarius simulation. Springel et al 2008. WMAP-1

## Central slope is very close to -1

For normal galaxies it does not matter: baryons dominate in those regions and affect DM

Stadel et al 2009



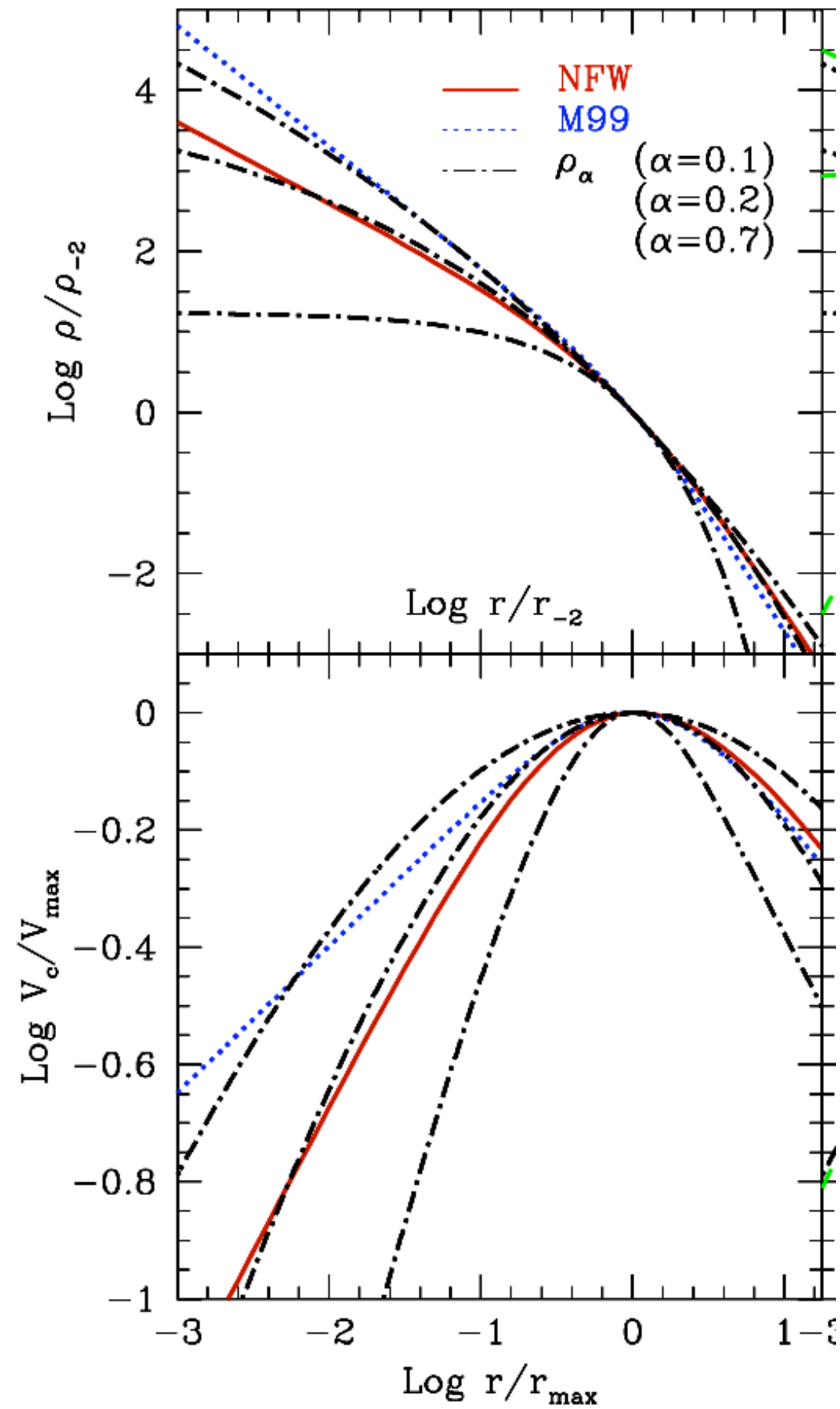
# Einasto

$$\rho_{-2} = \rho_s/4$$

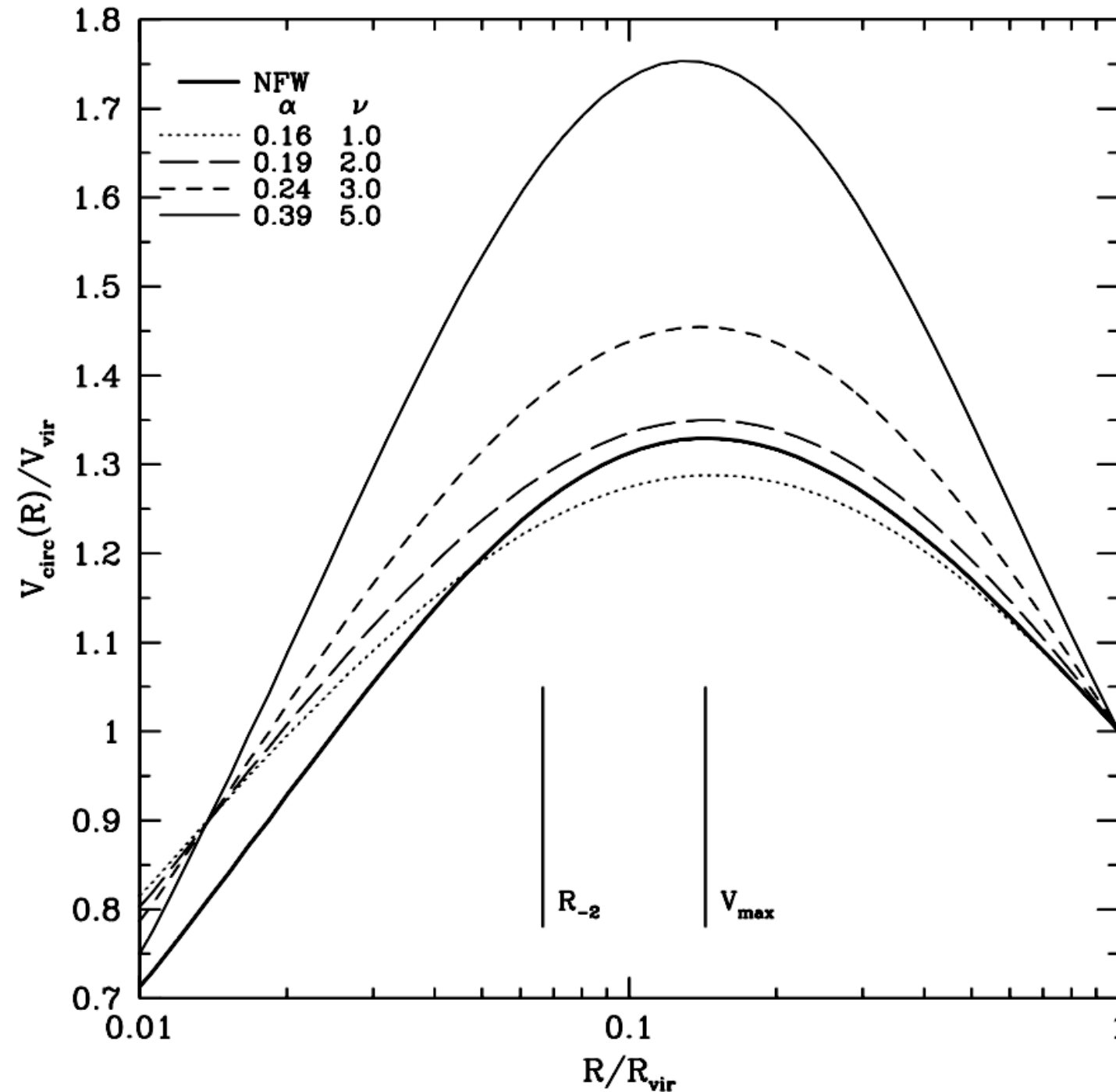
$$r_{-2} = r_s.$$

$$\alpha = 0.2$$

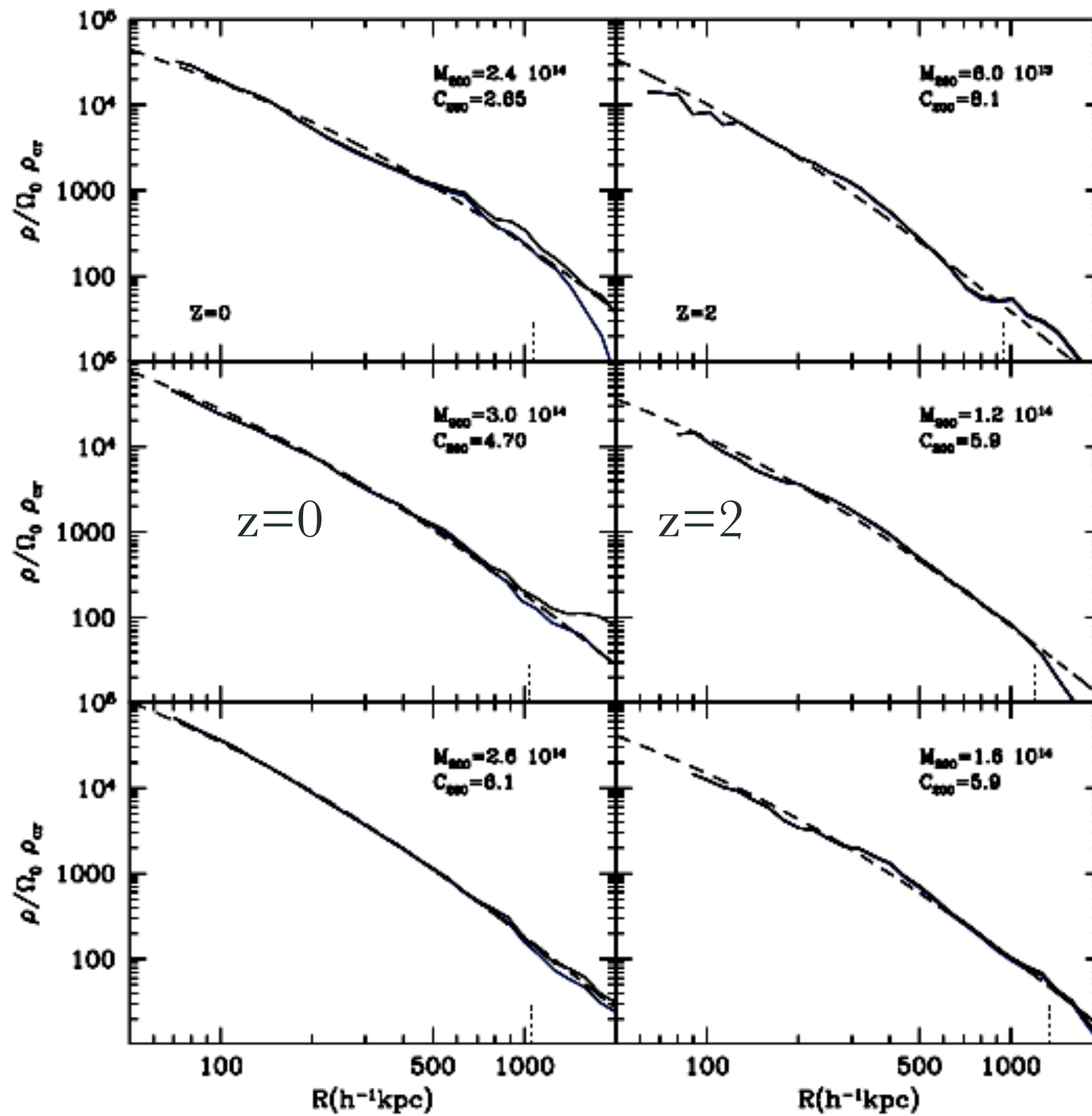
$$\ln(\rho_\alpha/\rho_{-2}) = (-2/\alpha)[(r/r_{-2})^\alpha - 1].$$



## Halos with the same viral radius



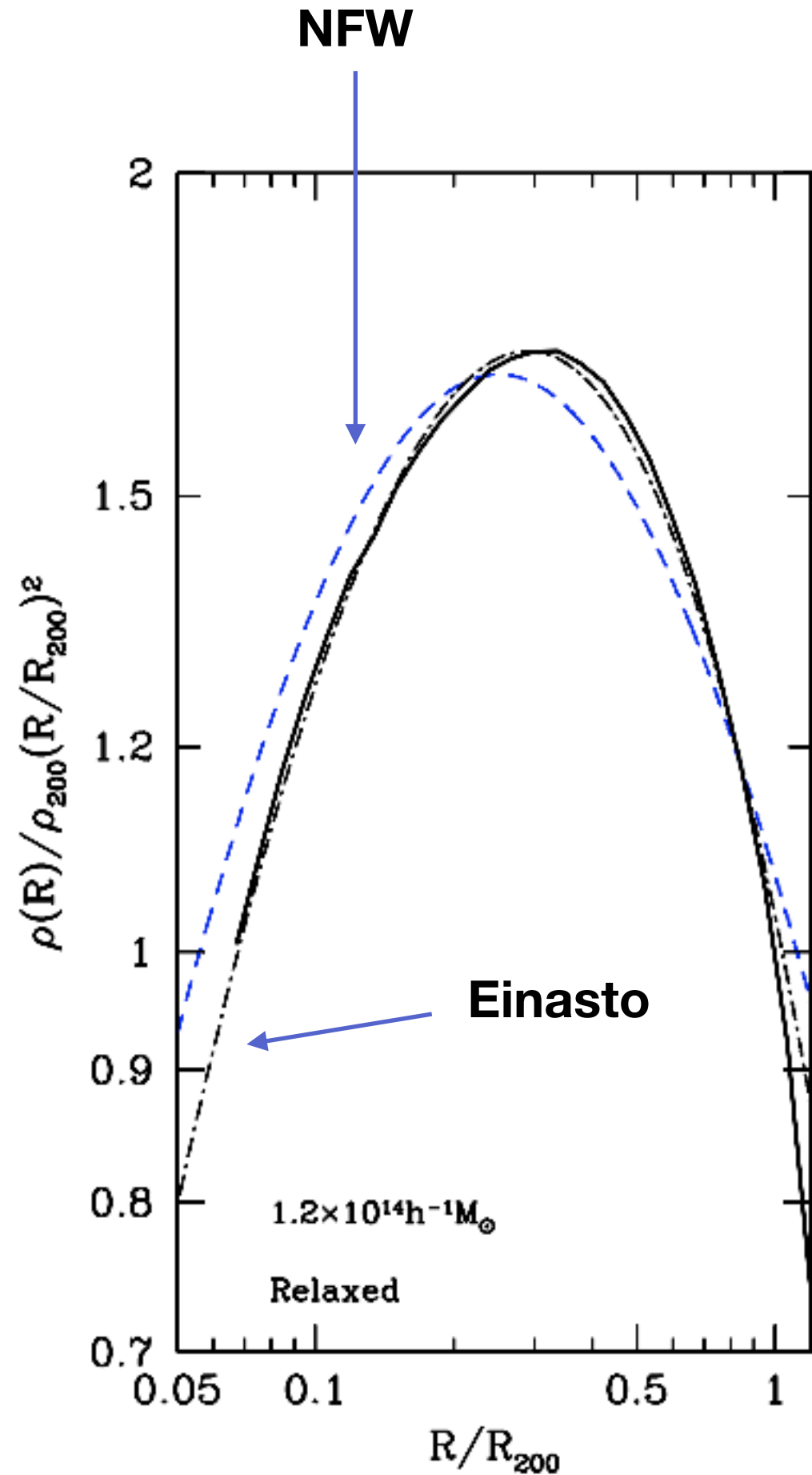
Comparison the NFW halo profile with the Einasto profiles with different parameters  $\alpha$ . Halos were fixed to have the same virial mass, and the same radius  $r_{-2}$  where the slope of the density profile is equal to  $d \log(\rho)/d \log(R) = -2$ . In cosmological simulations the parameter  $\alpha$  depends on the peak height  $\nu$  with larger  $\nu$  (and, thus, larger mass  $M$ ) corresponding to larger parameters  $\alpha$ . The ratio of the maximum circular velocity to the virial velocity  $V_{\text{circ}}/V_{\text{vir}}$  is related with halo concentration for any profile.

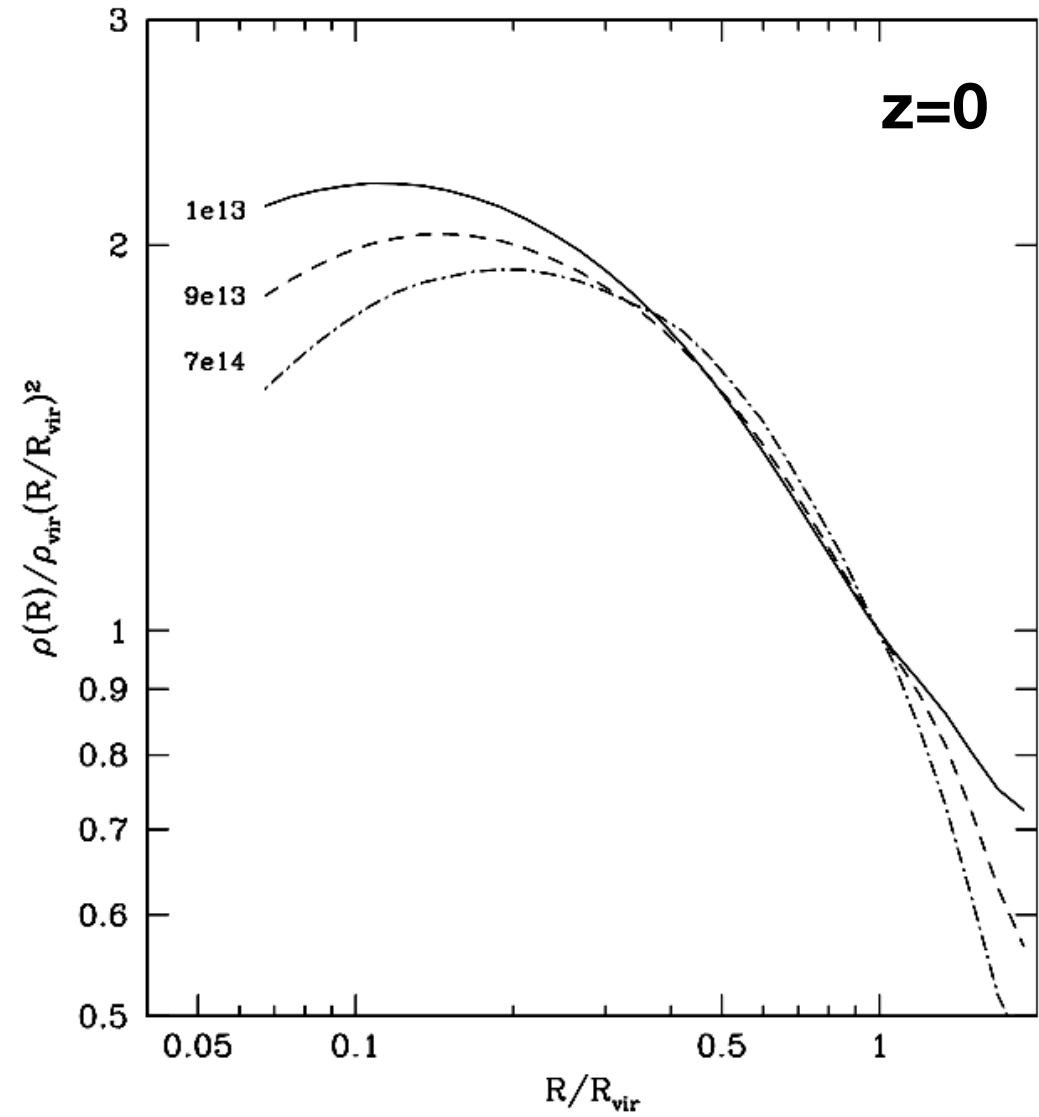
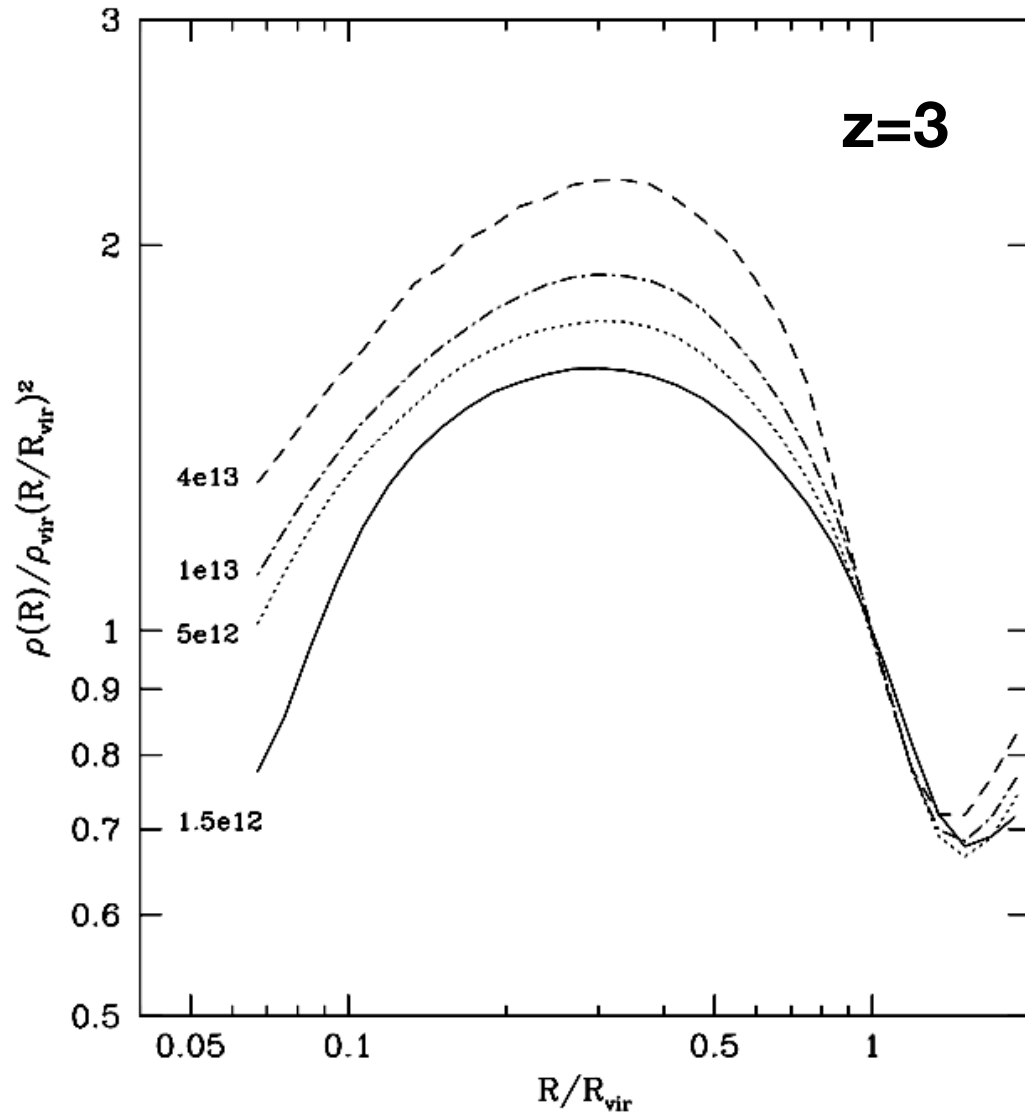


**Figure 3.** Examples of density profiles for cluster-size haloes (full curves) and their fits (dashed curves) using concentrations obtained with the ratios of the maximum circular velocity  $V_{\text{max}}$  to the halo velocity  $V_{200}$ . Panels on the left are for redshift  $z = 0$  and the right-hand panels are for  $z = 2$ . Each panel shows two full curves: the density profile of all particles (upper curve) and only bound particles (lower curve). Vertical dotted lines show the outer radius of bound particles.

# Very massive halos

Density profiles of halos with mass  $M_{200} \approx 1.2 \times 10^{14} h^{-1} M_{\odot}$  at  $z = 1.5$  (full curves). Dot-dashed curves show Einasto fits, which have the same virial mass as halos in the simulation. The NFW profiles (dashed curves) do not provide good fits to the profiles and significantly depend on what part of the density profile is chosen for fits.





Median density profiles of relaxed halos at different redshifts and masses in N-body simulations. Profiles are normalized to have the same density at the virial radius. The left panel is for halos at  $z = 3$ : halos with larger mass are clearly more concentrated than halos with smaller masses. Similar to Einasto profiles in Figure 7, value of  $r_{-2}$  radius almost does not change with halo mass, which indicates that the increase in the concentration is mostly due to the increase in shape parameter  $\alpha$ . The right panel shows profiles of halos at  $z = 0$ . Note that the trend with mass is different: more massive halos are less concentrated and  $r_{-2}$  radius decreases with decreasing mass.

# Densities and velocities at large distances

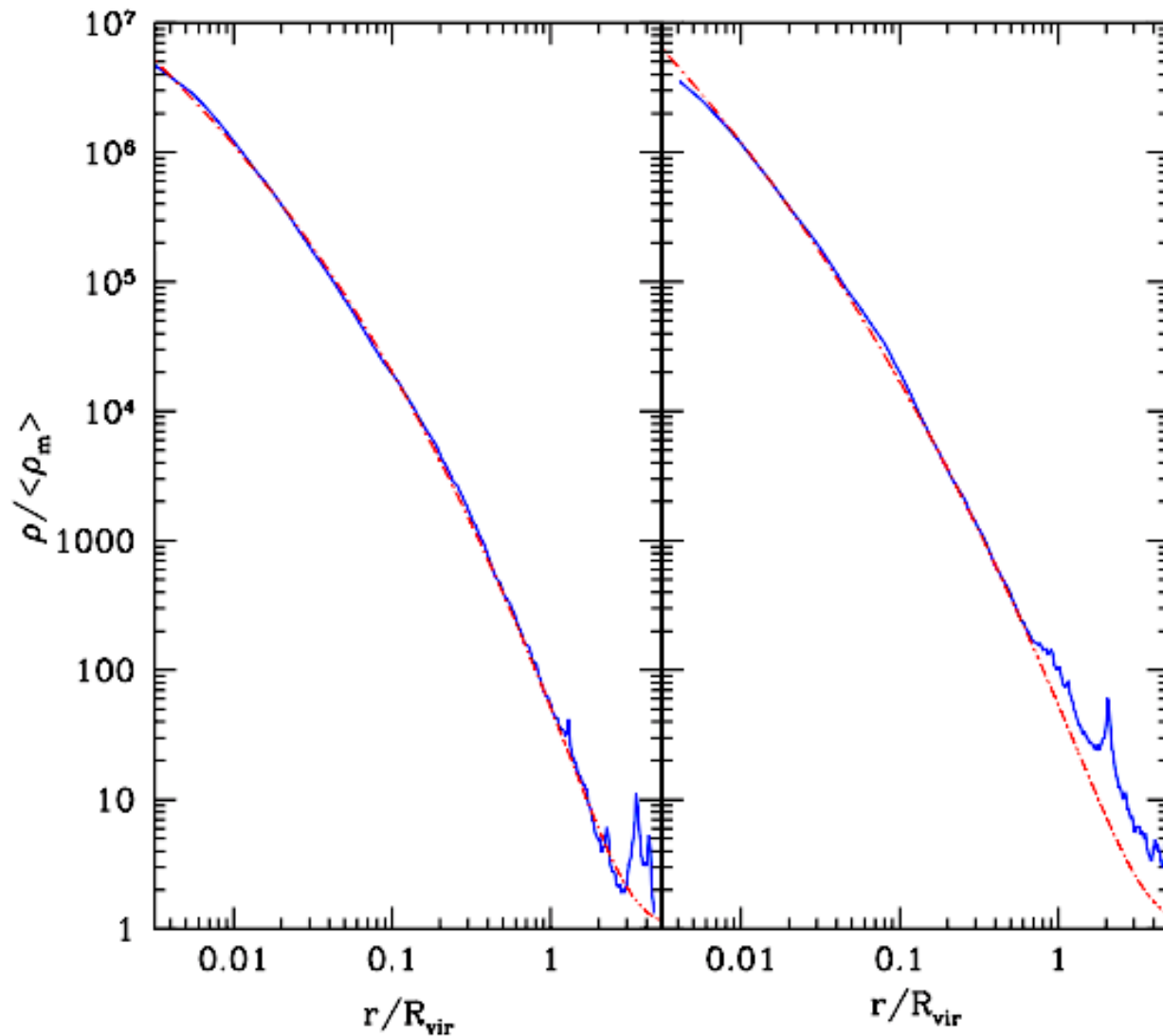
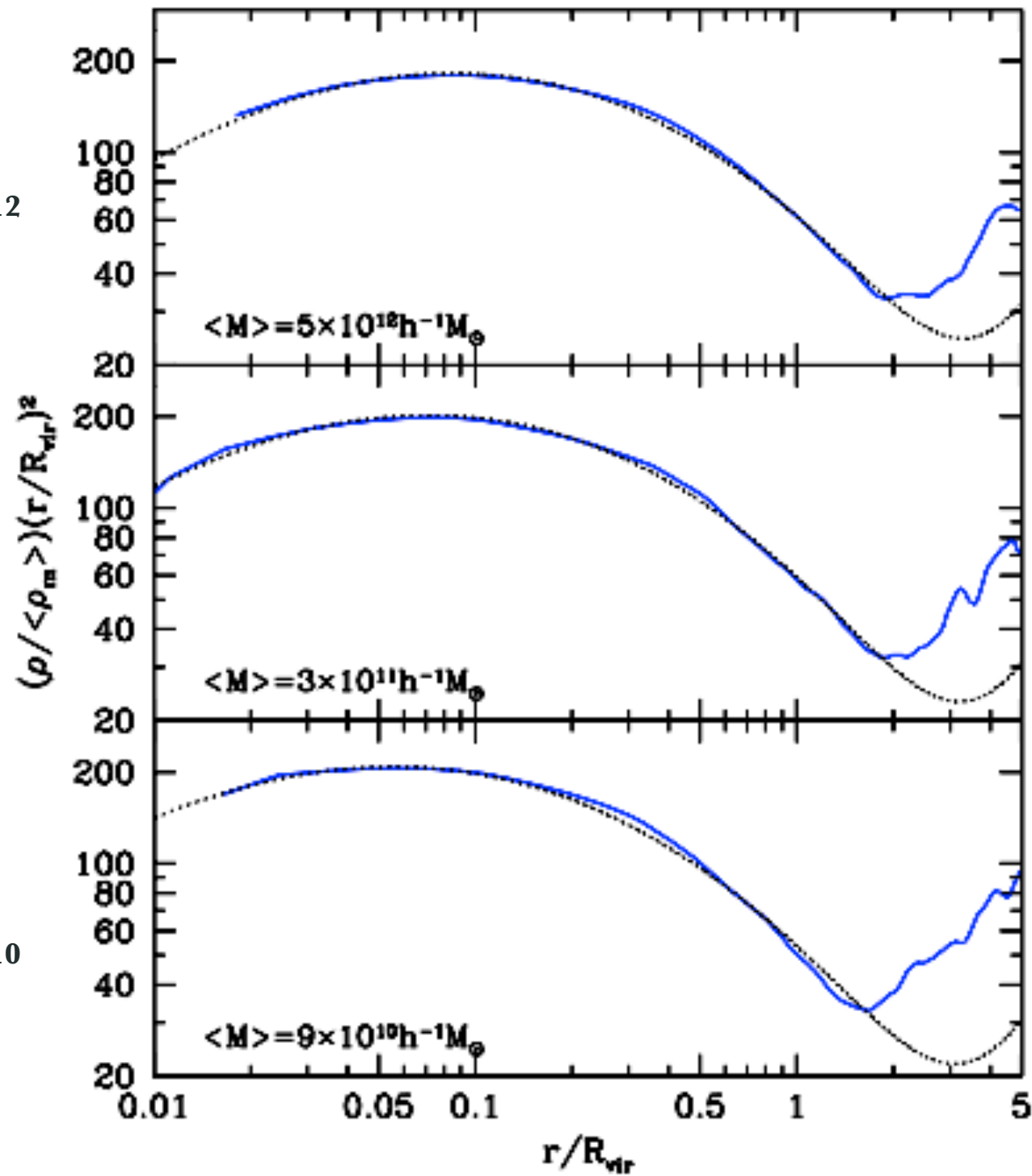


Fig. 1.— Dark matter density profiles of two dark matter halos (full curves) in the simulation Box20. The halos have virial masses of  $1.4 \times 10^{12} h^{-1} M_{\odot}$  (left panel) and  $2.6 \times 10^{11} h^{-1} M_{\odot}$  (right panel). The larger halo has a neighbour at  $3.5 R_{\text{vir}}$  which is the halo on the right panel. This smaller halo is responsible for the spike at large radii in the density profile. In turn, the halo on the right panel has its own smaller neighbour at  $2R_{\text{vir}}$  observed as a spike and an extended bump in the density profile. The dashed curves show the 3D Sersic profiles. The halo density profiles extend well beyond the formal virial radius with the Sérsic profile providing remarkably good fits. **Einasto**

$M=5 \times 10^{12}$

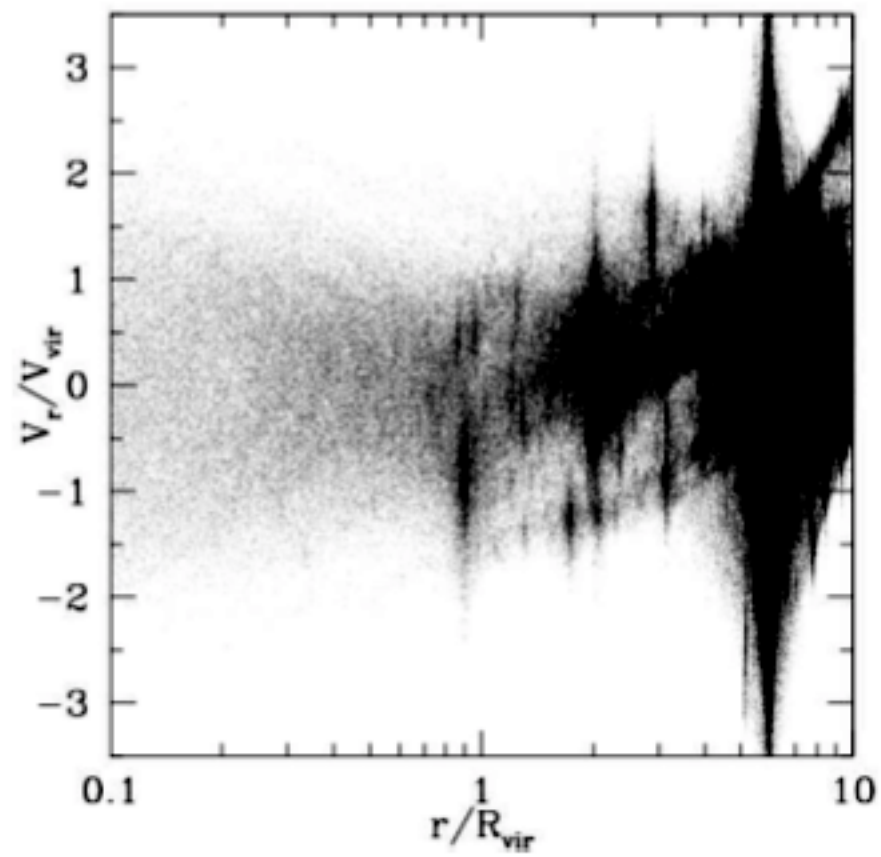


$M=9 \times 10^{10}$

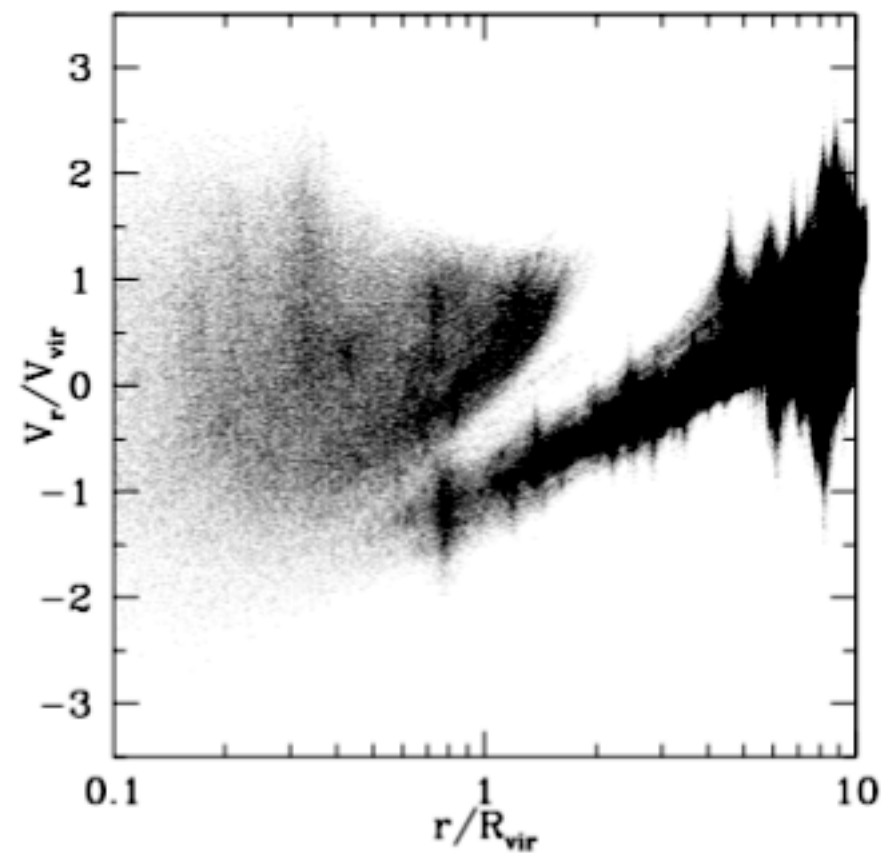
Fig. 3.— Average density profiles for halos with different virial masses. The 3D Sérsic profile provides very good fit with few percent errors within  $2R_{\text{vir}}$ . Even at  $3R_{\text{vir}}$  the error is less than 20-30 percent. The density profiles are well above the average density of the Universe throughout all the radii.

**3d Sersic = Einasto**

Phase-space diagram for the particles in dark matter halos



$M_{vir} = 3 \cdot 10^{11} M_{sun}$



$M_{vir} = 1.5 \cdot 10^{15} M_{sun}$

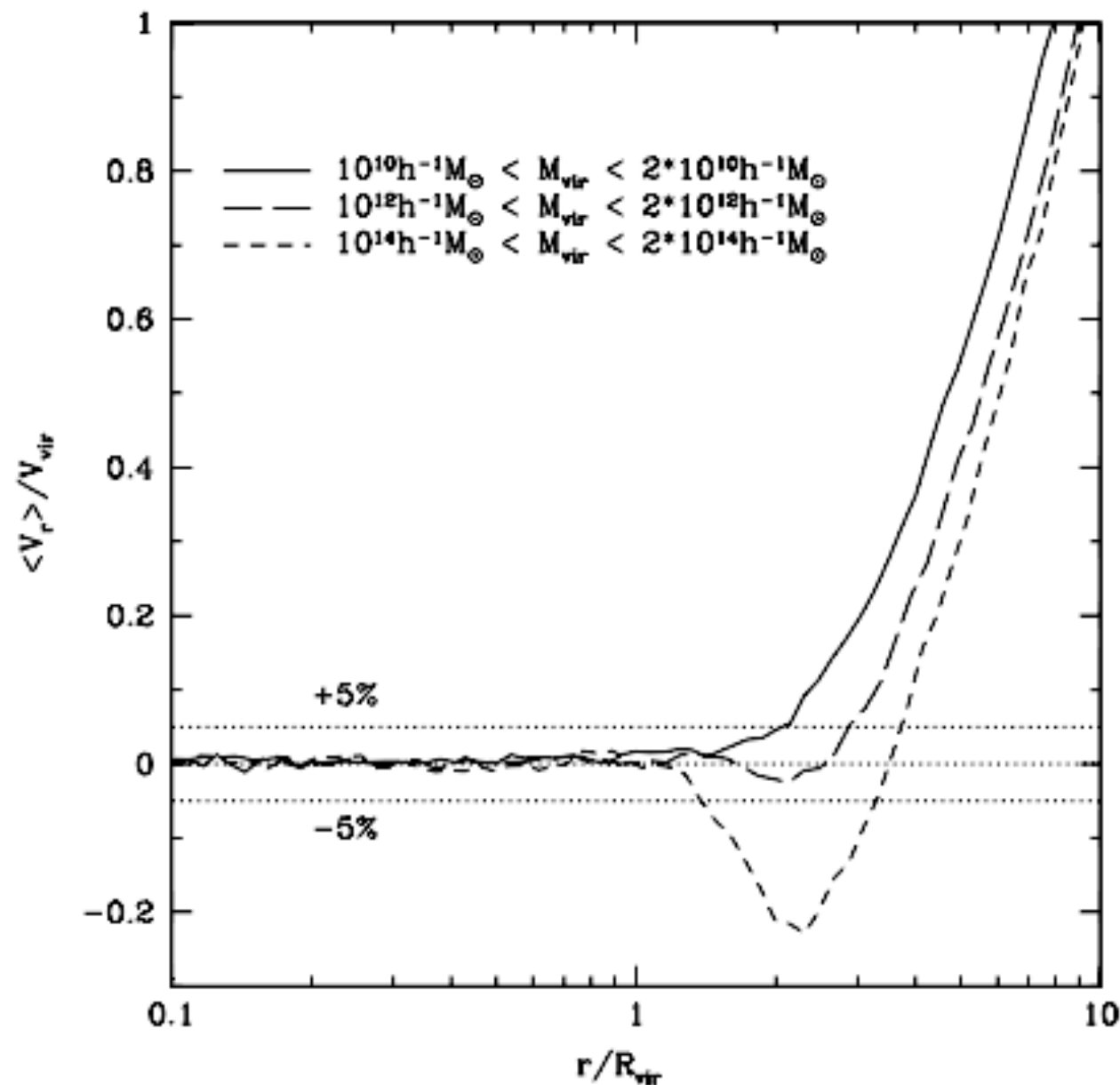
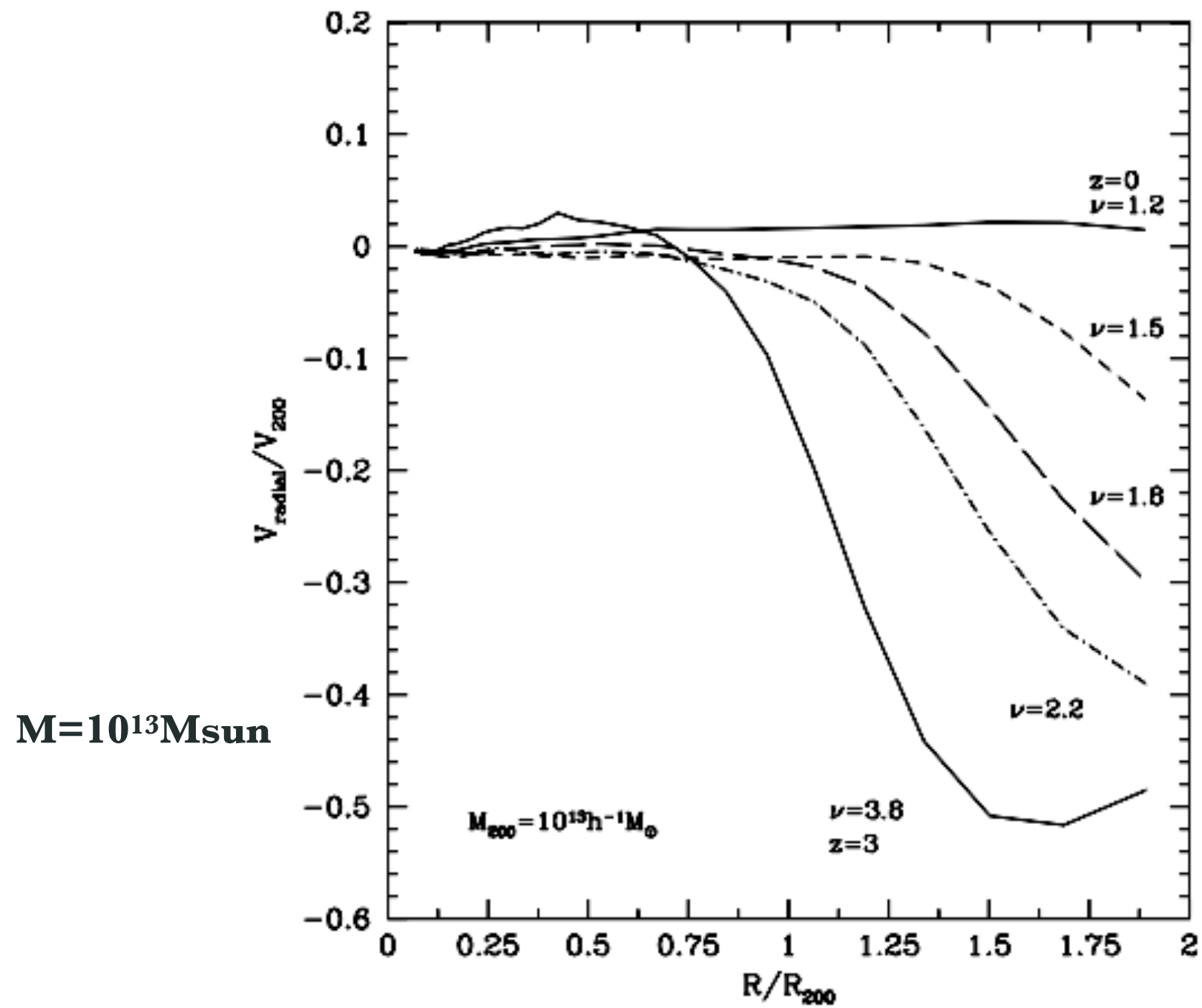


**Figure 4.** Mean radial velocity for three different mass bins. The profiles were obtained by averaging over hundreds of distinct haloes on each mass bin. In dotted line is shown the selected threshold delimiting the static region (5 per cent of the virial velocity). Cluster-size haloes display a region with strong infall (dashed line). On the contrary, low-mass haloes (solid line) and galactic haloes (long-dashed line) do not show infall at all but a small outflow preceding the Hubble flow.

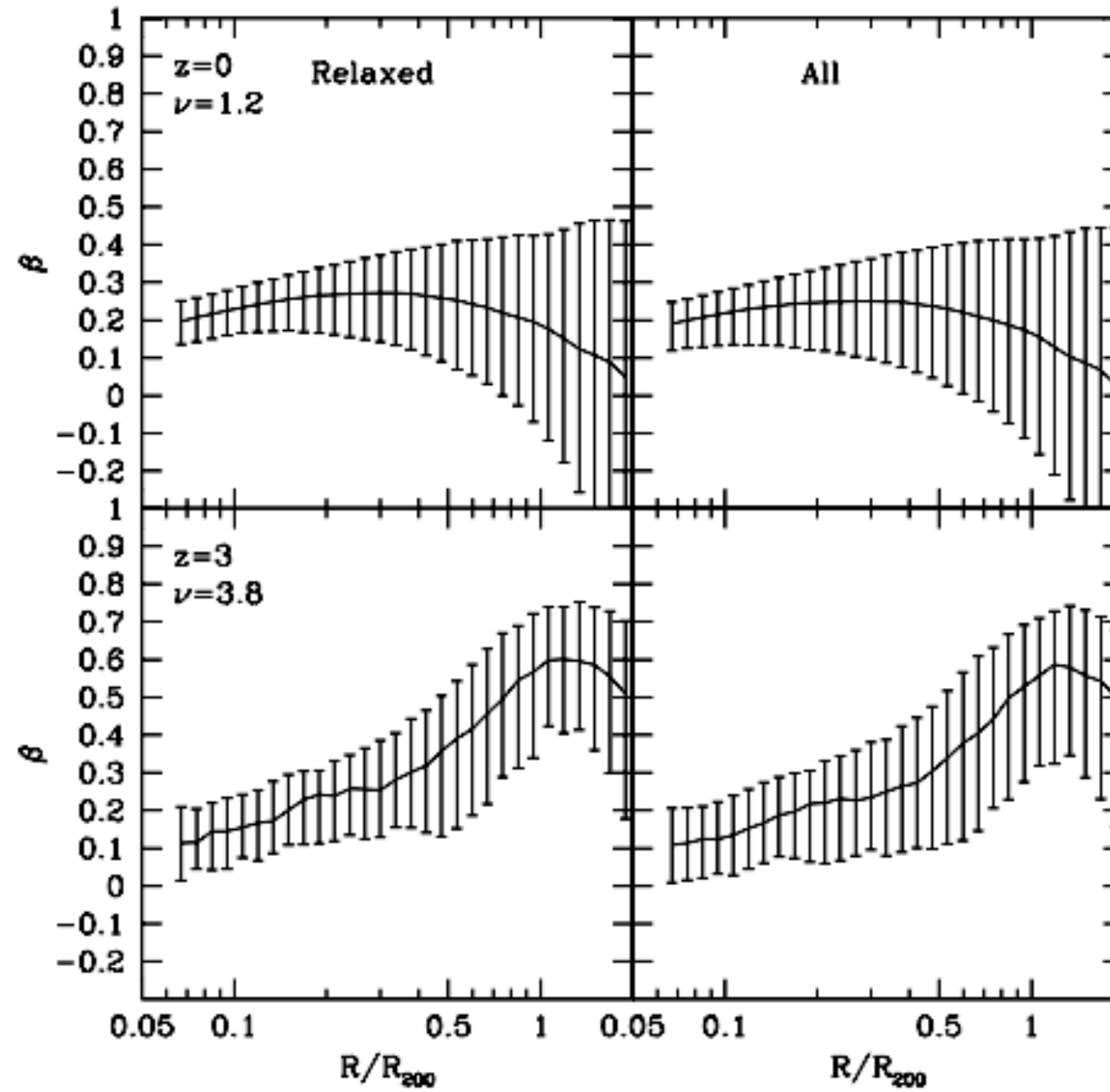
# Infall velocities on halos.

$$\nu = \text{peak height} = \delta_{\text{cr}}/\sigma$$



# Velocity anisotropy

$M=10^{13}M_{\text{sun}}$



$\delta_{\text{cr}}/\sigma$

$$\beta = 1 - \frac{\sigma_t^2}{\sigma_r^2},$$

where  $\sigma_r^2$  is the radial velocity dispersion and  $\sigma_t^2$  is the tangential velocity dispersion.

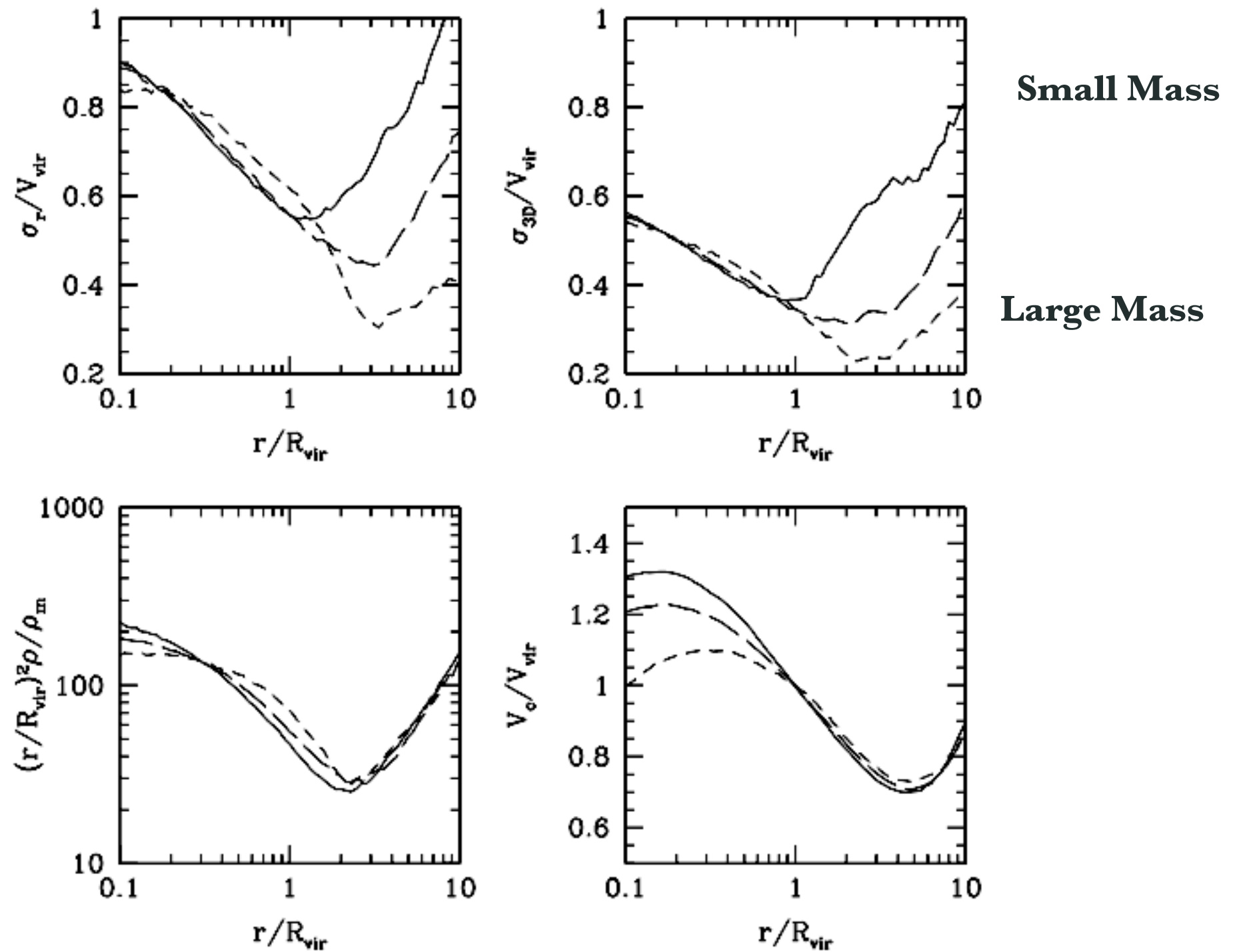
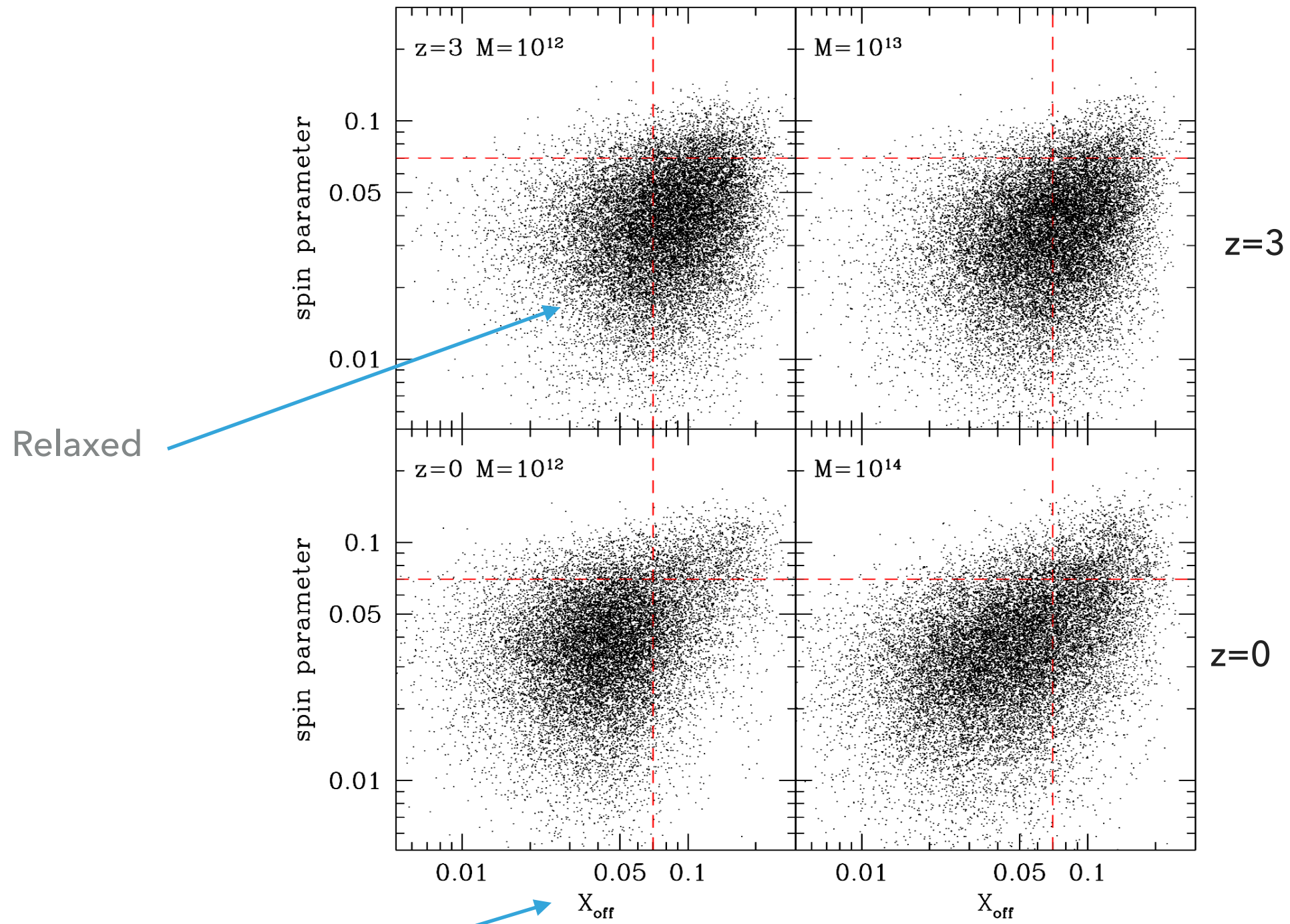
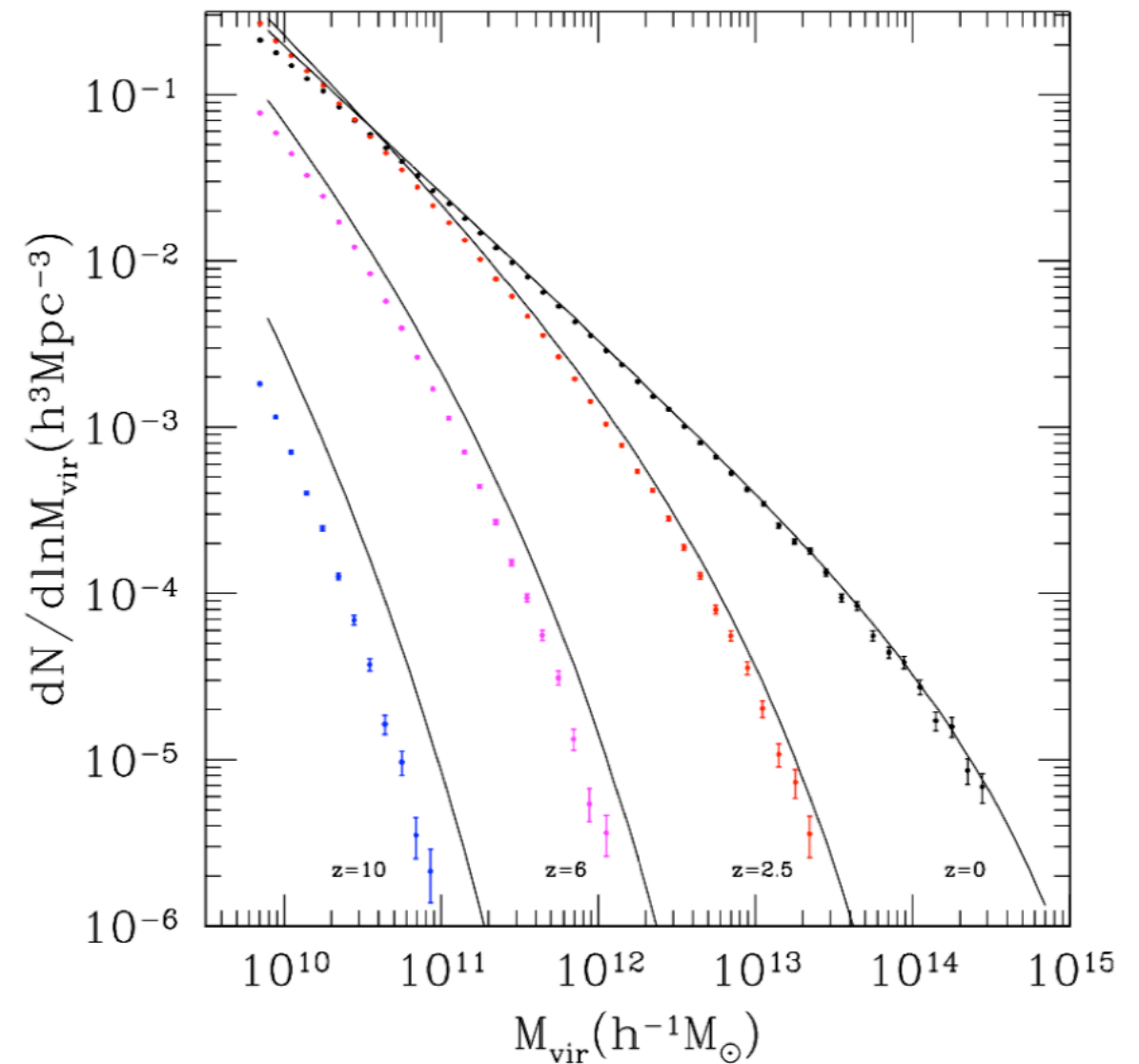
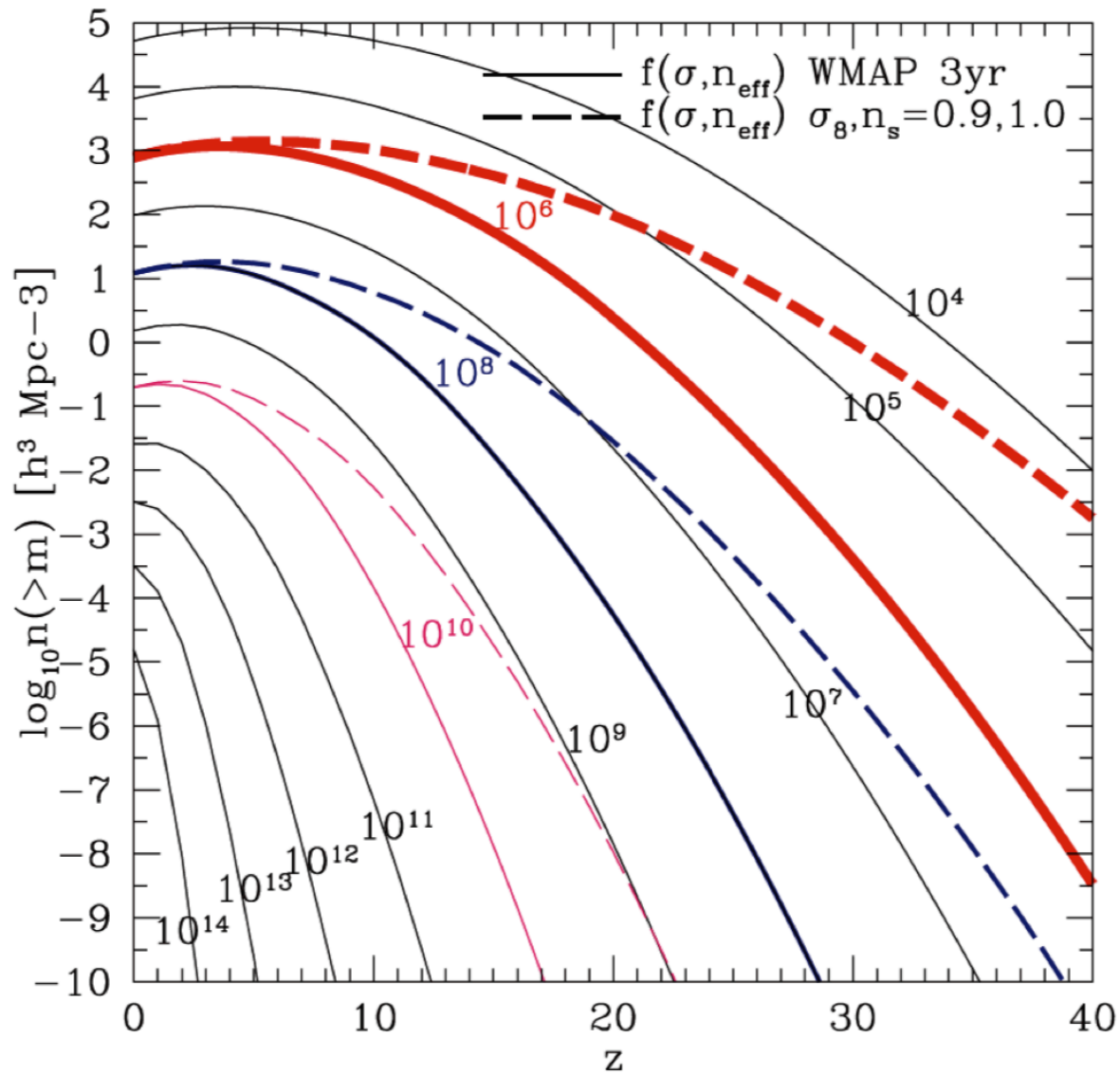


**Figure 5.** Median profiles for the same halo mass bins as in Figure 4. These profiles show how the behaviour of haloes depends on the halo mass. Top left panel: radial velocity dispersion. Top right: 3D velocity dispersion. Bottom left: density profile. Bottom right: Circular velocity profile. The different line styles represent the same mass bins as in Figure 4.



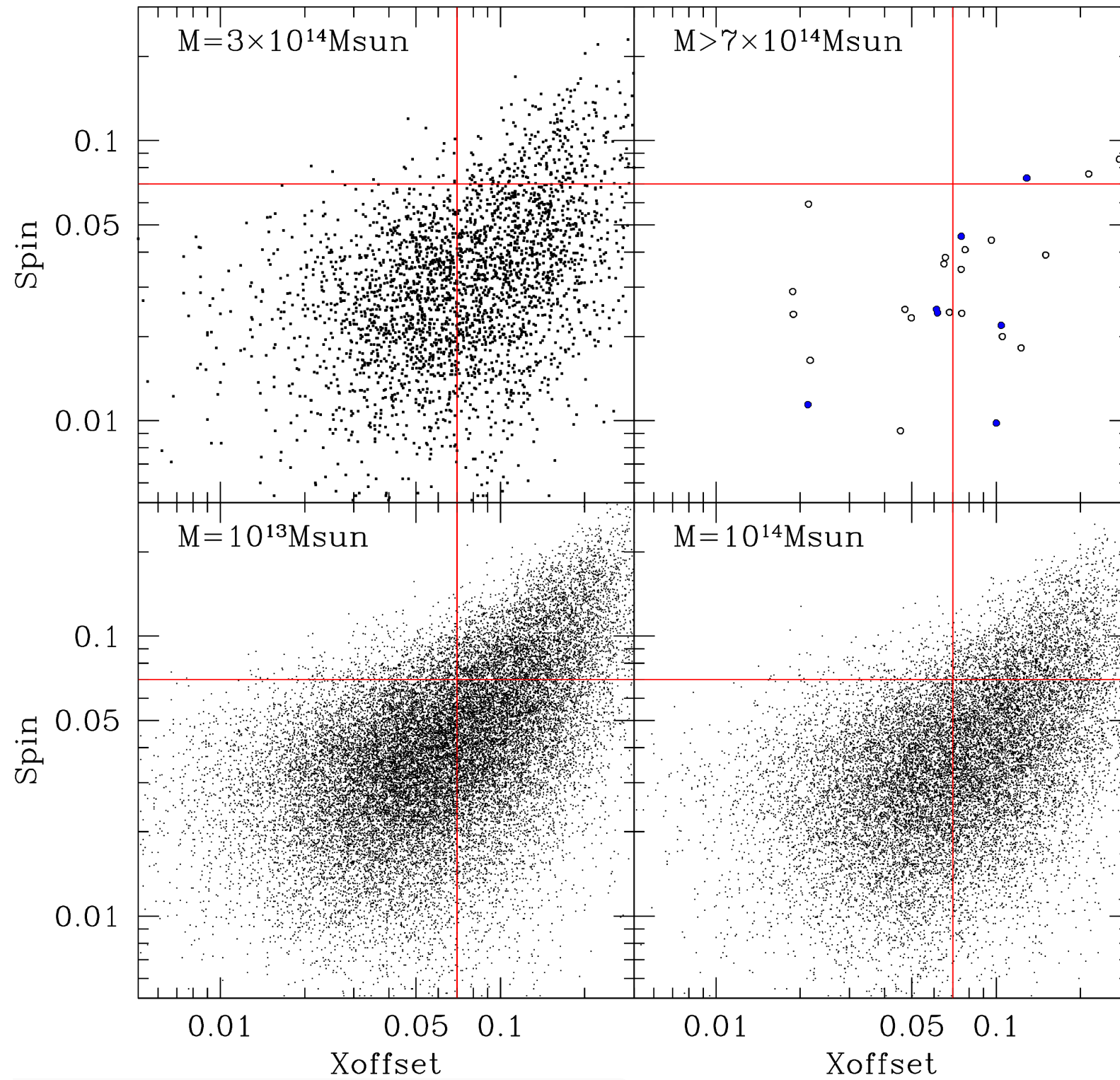
## Evolution of halo mass function with redshift



Uchuu:  $2\text{Gpc}/h$  volume  $\Rightarrow$  one object corresponds to  $n = 1.2 e^{-10} \text{Mpc}^{-3}$

at  $z=0.83$  we have  $\sim 20$  halos with  $M > 7e14 M_{\text{sun}} \Rightarrow$   
 $n(>m) = 2.5e-9 \text{Mpc}^{-3}$

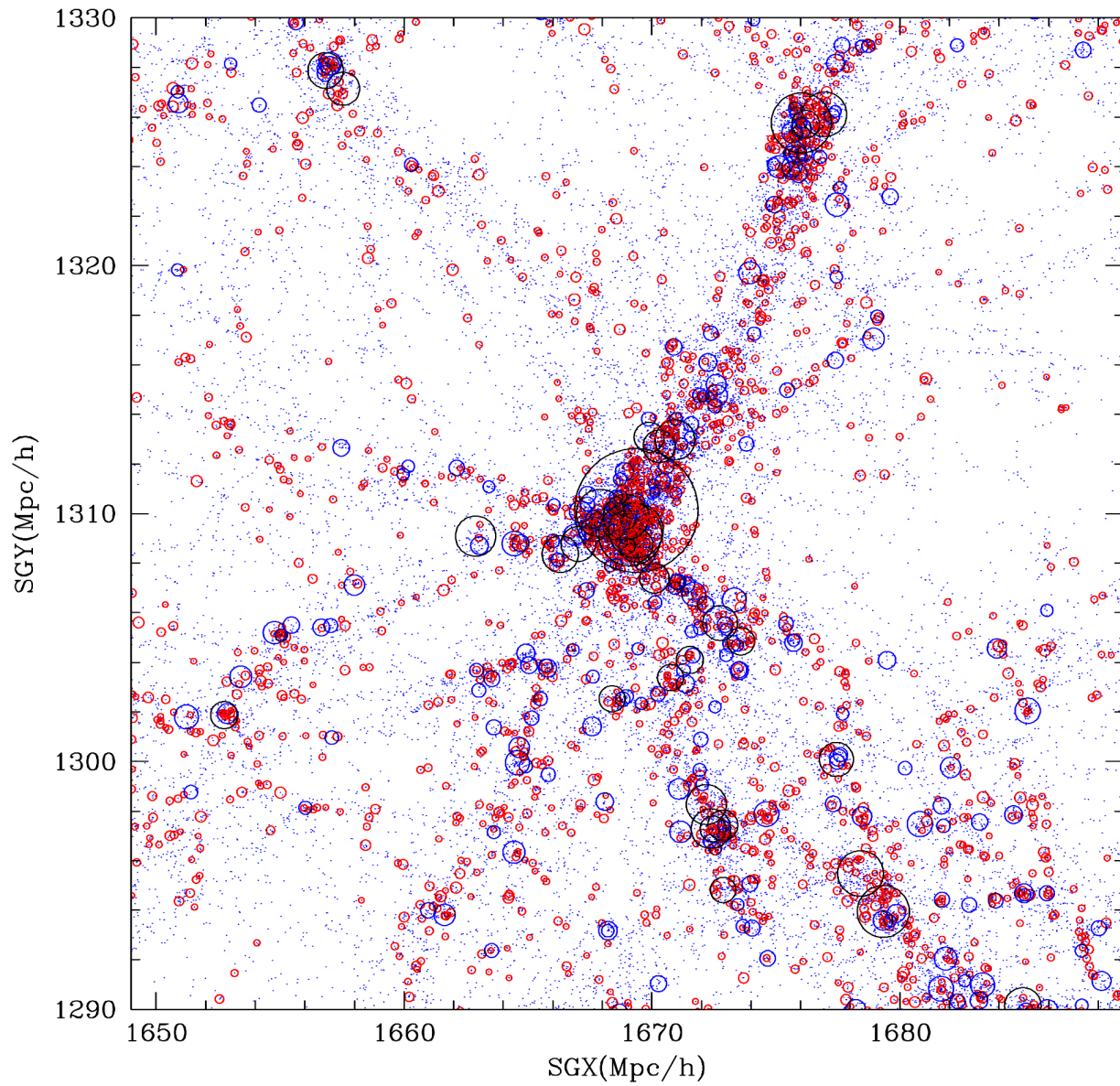
# UCHUU: 2GPC SIMULATION WITH 2TRILLION PARTICLES. $Z = 0.9$



# WHAT THIS ABOUT: LARGEST CLUSTERS AT Z=1

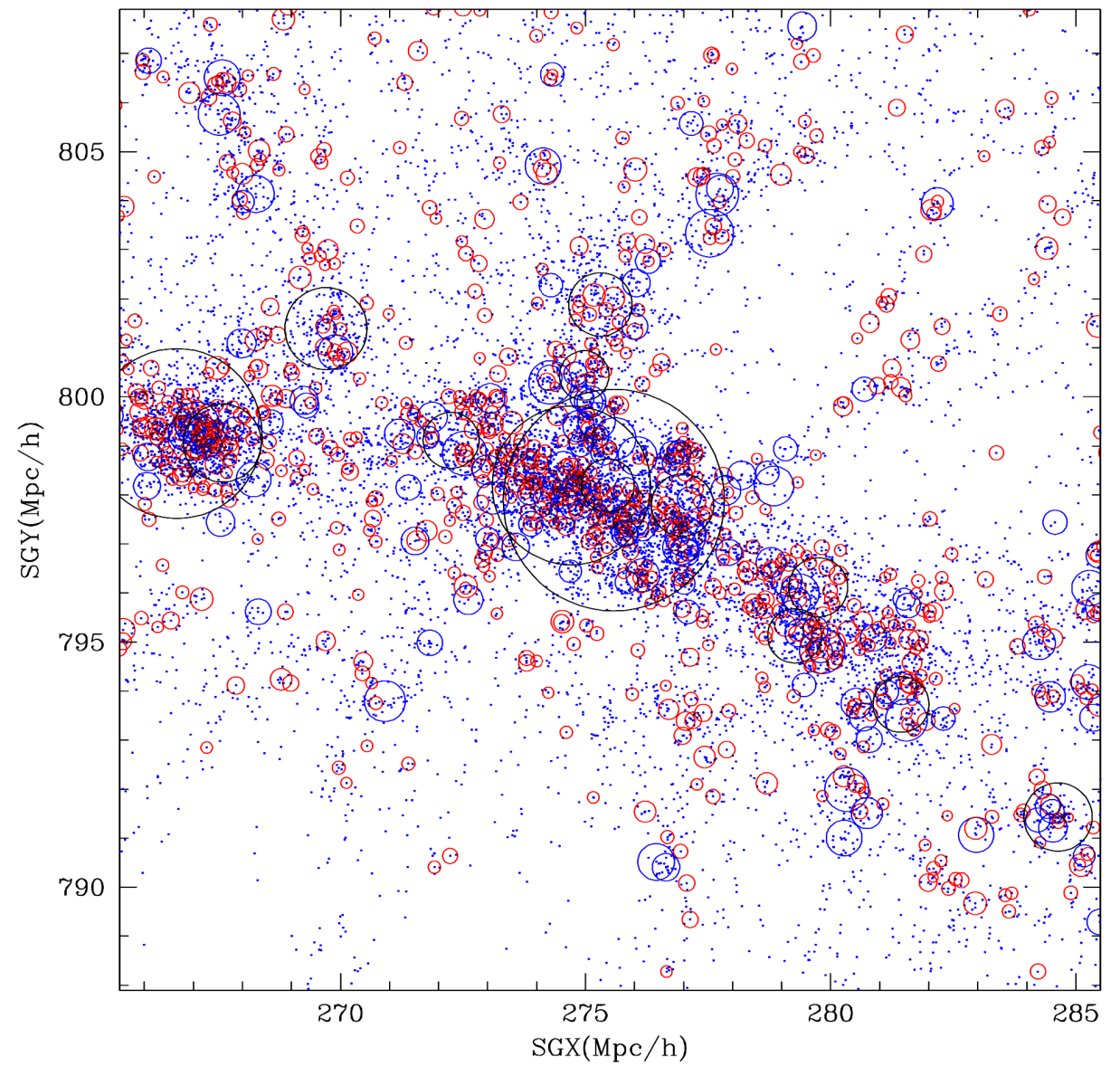
“Non relaxed” cluster

$M_{\text{vir}}=1.1e15M_{\text{sun}}$   $\lambda=0.01$   $X_{\text{offset}}=0.10$   $z=0.87$

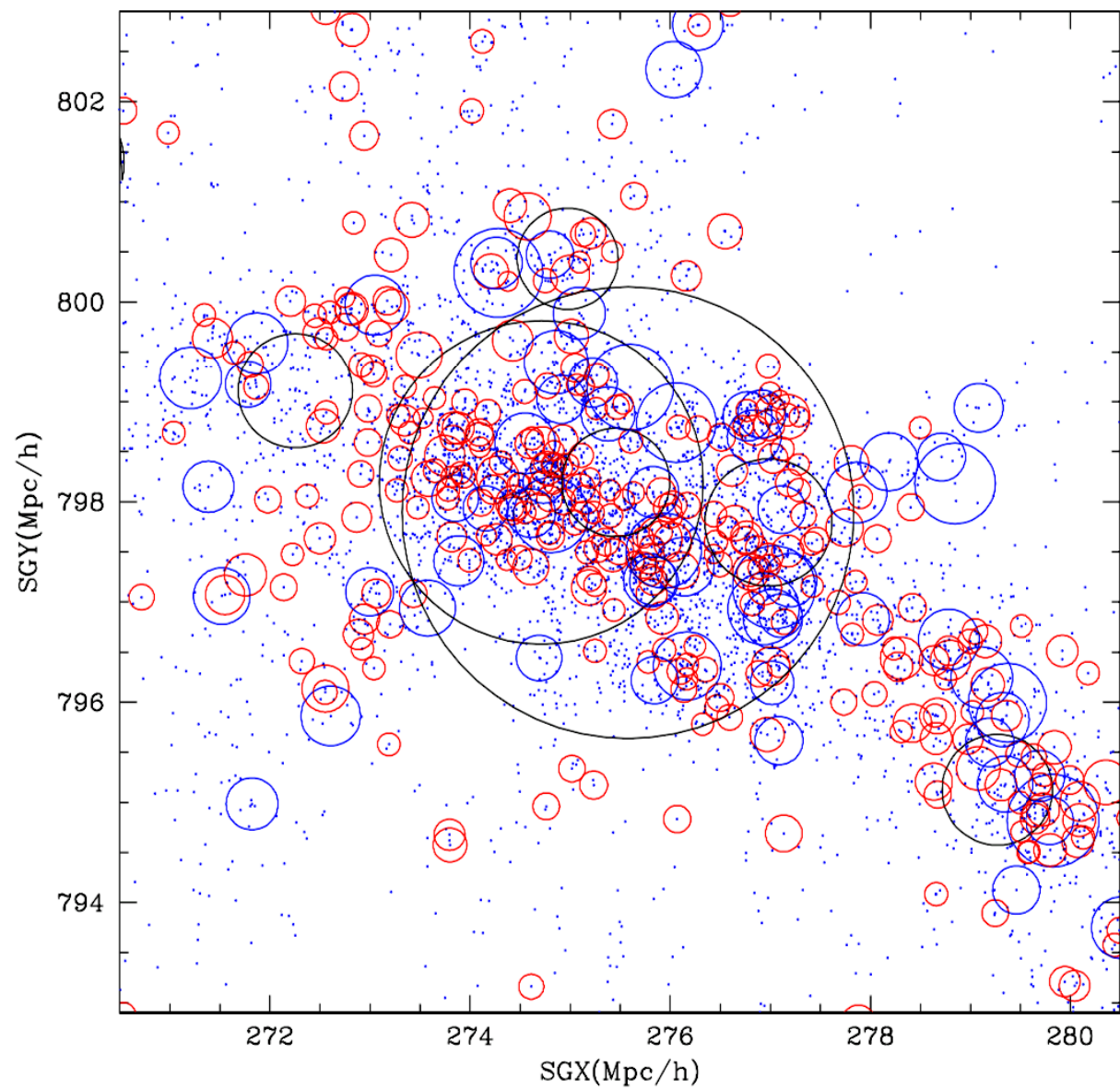


“Relaxed” cluster

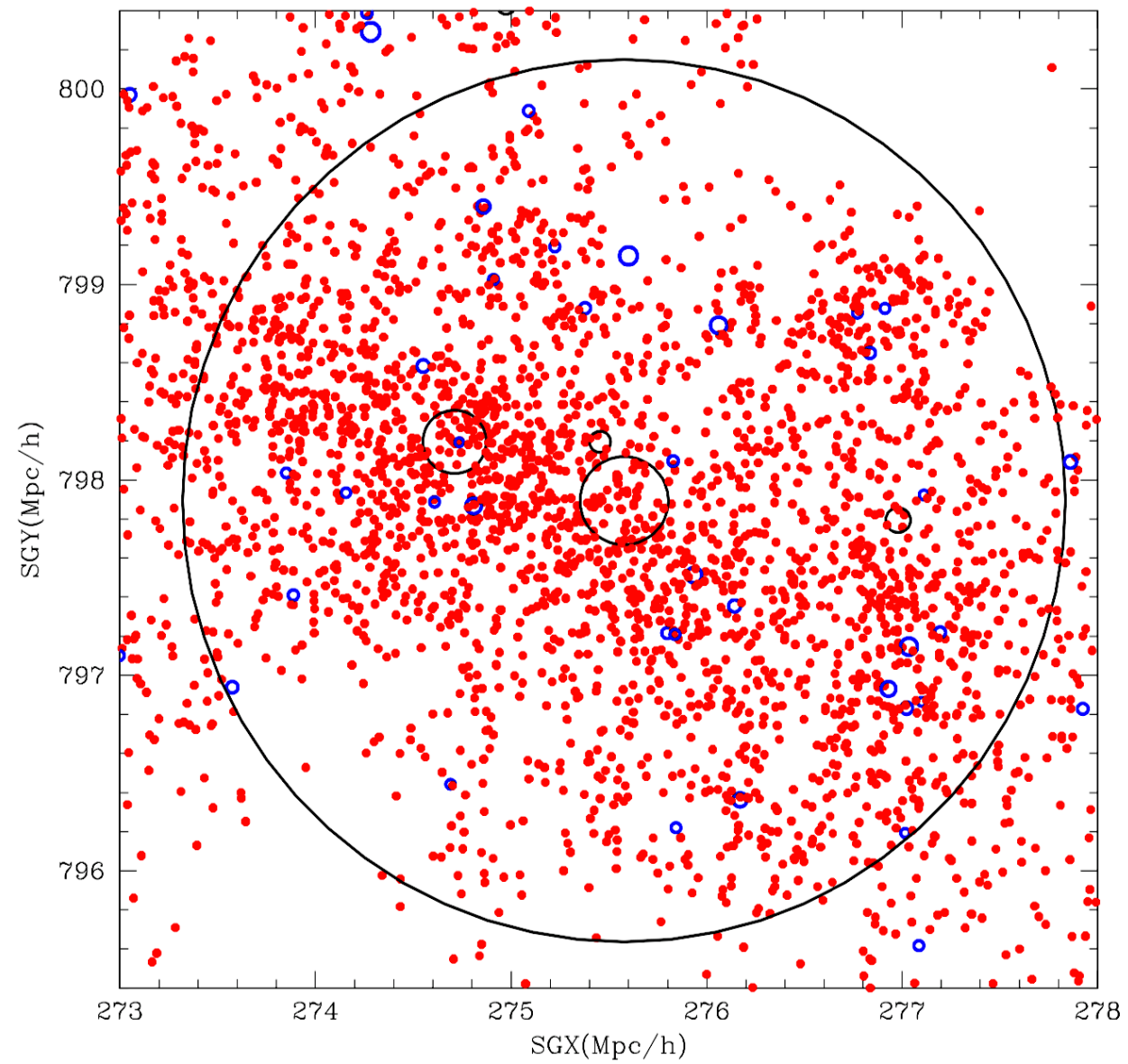
$M_{\text{vir}}=8.6e15M_{\text{sun}}$   $\lambda=0.036$   $X_{\text{offset}}=0.065$   $z=0.87$



$M_{\text{vir}}=8.6e14\text{Msun}$   $\lambda=0.036$   $X_{\text{offset}}=0.065$   $z=0.87$

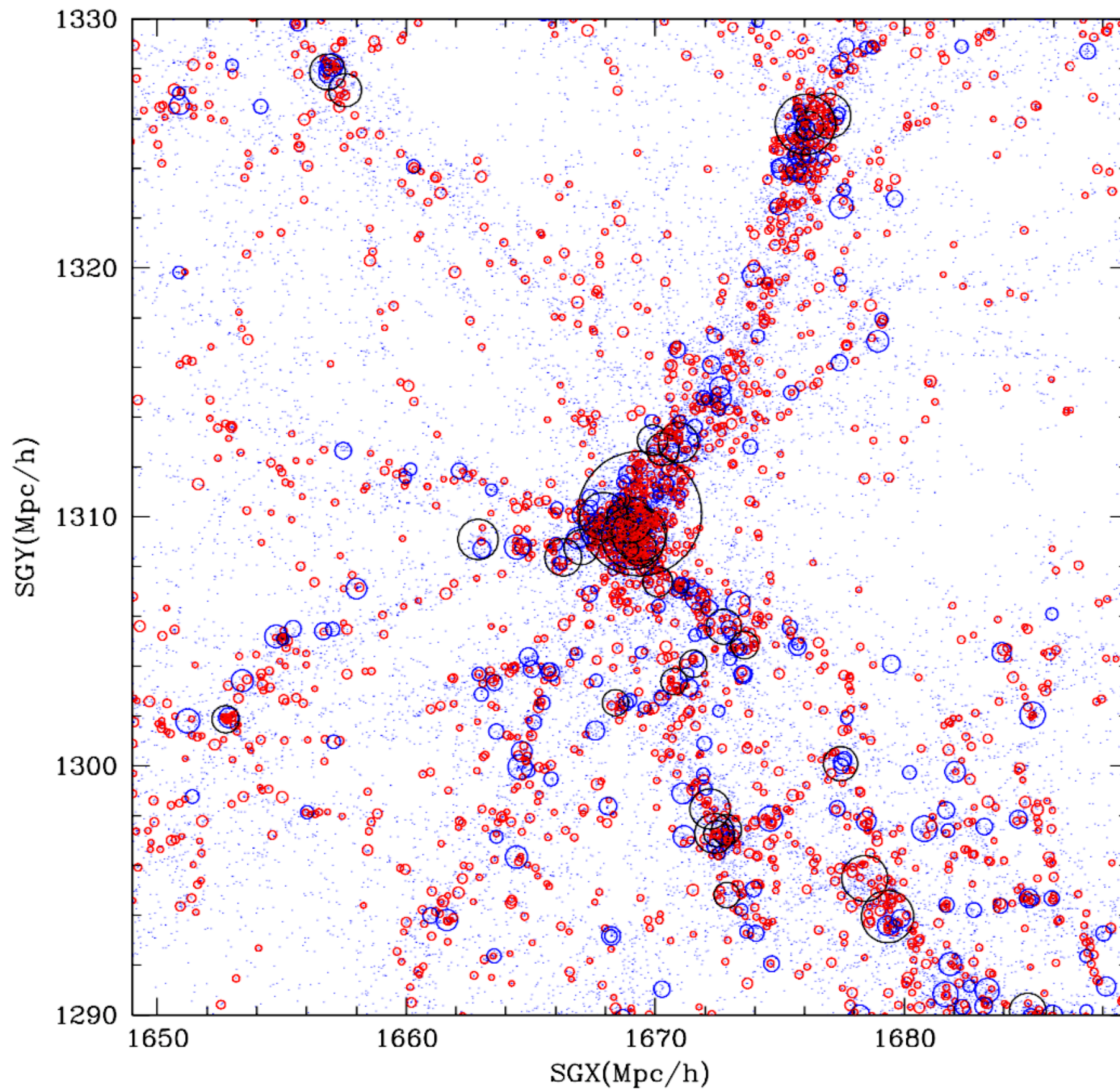


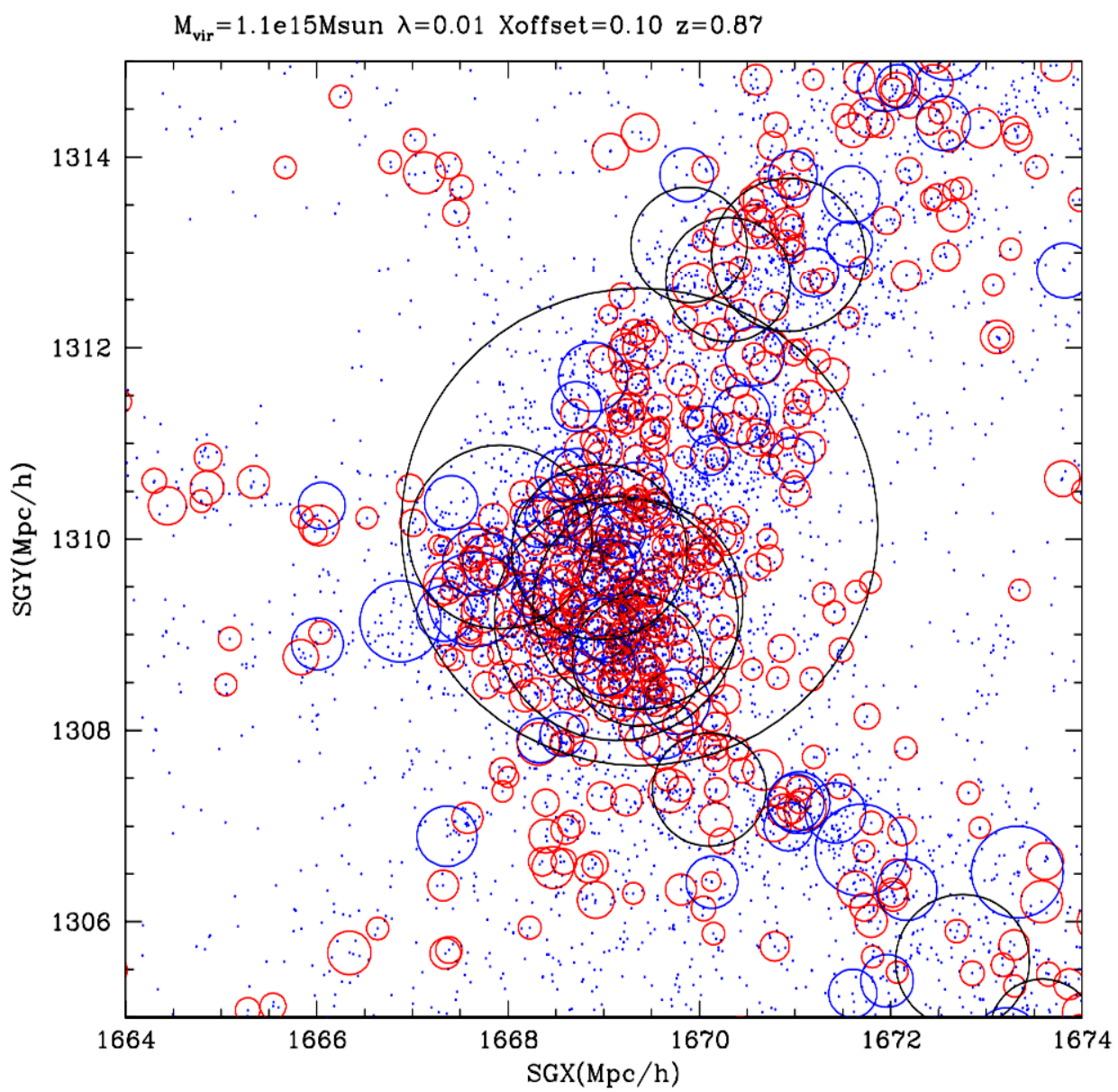
$M_{\text{vir}}=8.6e14\text{Msun}$   $\lambda=0.036$   $X_{\text{offset}}=0.065$   $z=0.87$



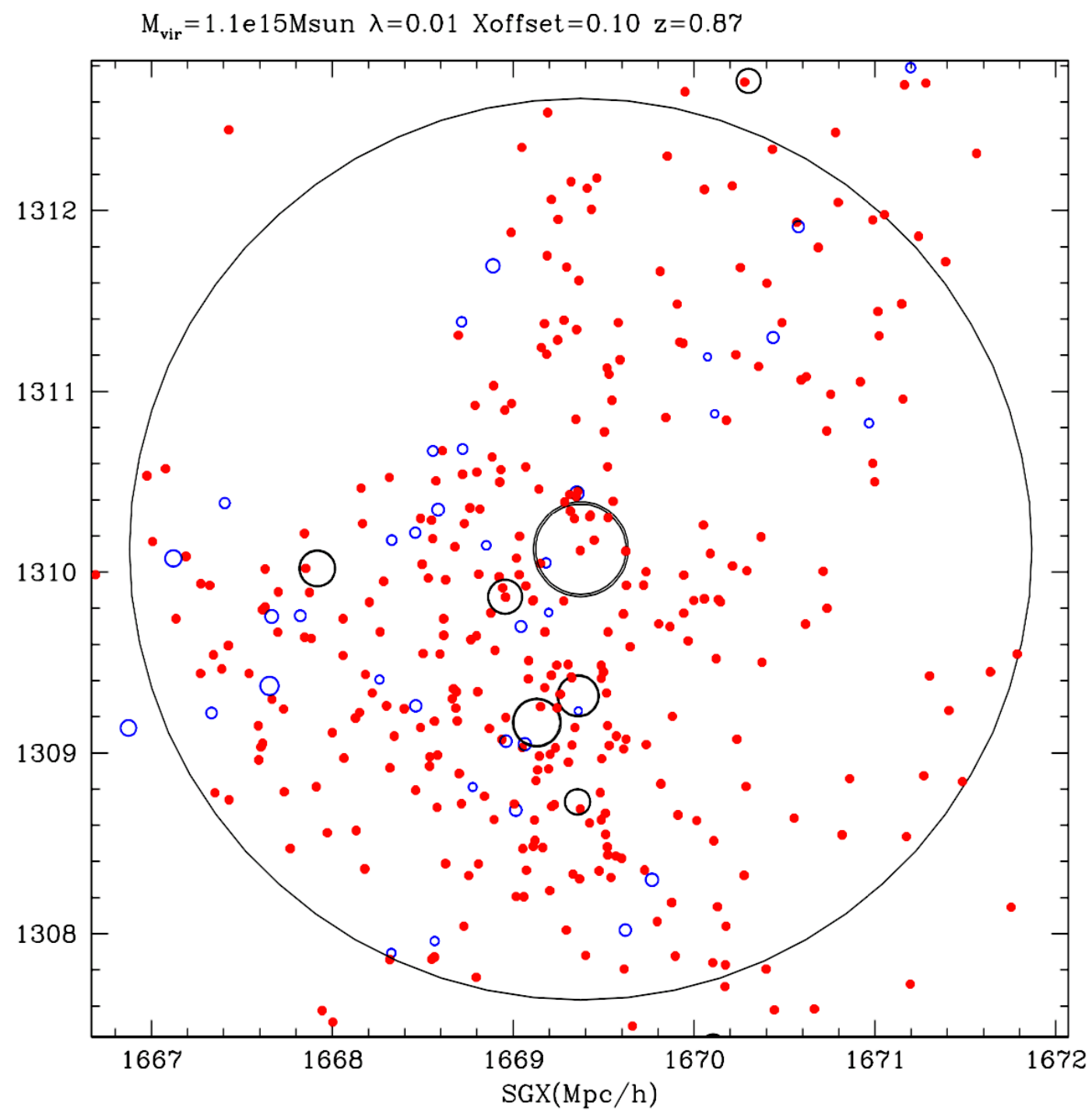
1/10 of Virial radii

$M_{\text{vir}}=1.1e15M_{\text{sun}}$   $\lambda=0.01$   $X_{\text{offset}}=0.10$   $z=0.87$





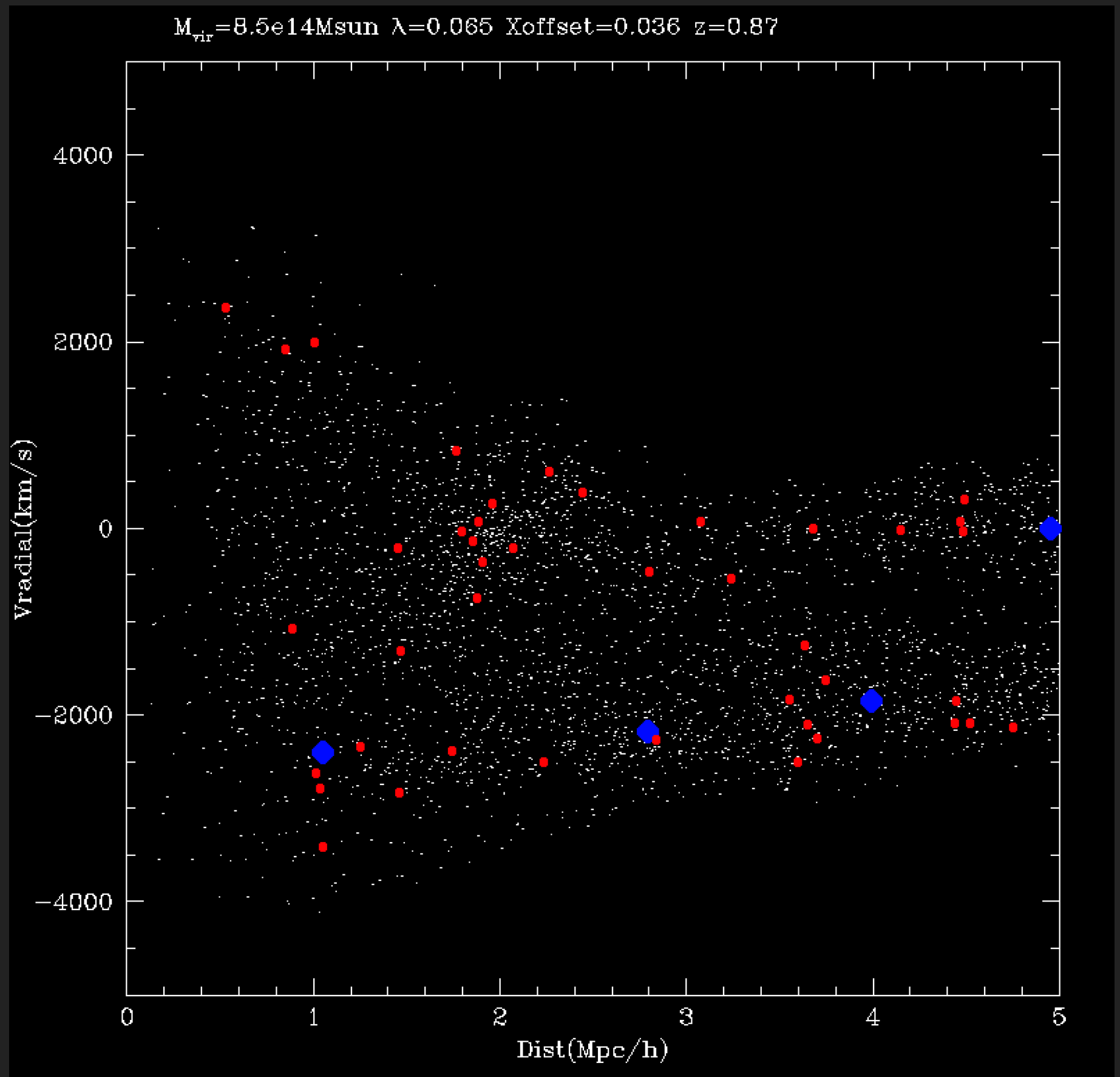
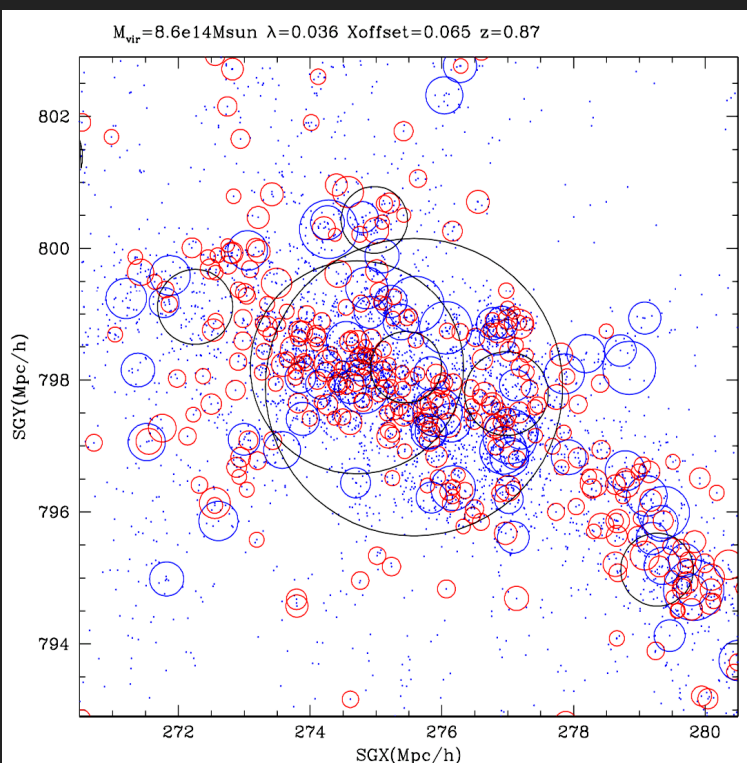
Virial radii



1/10 of Virial radii

Radial relative velocities  
for relaxed large cluster

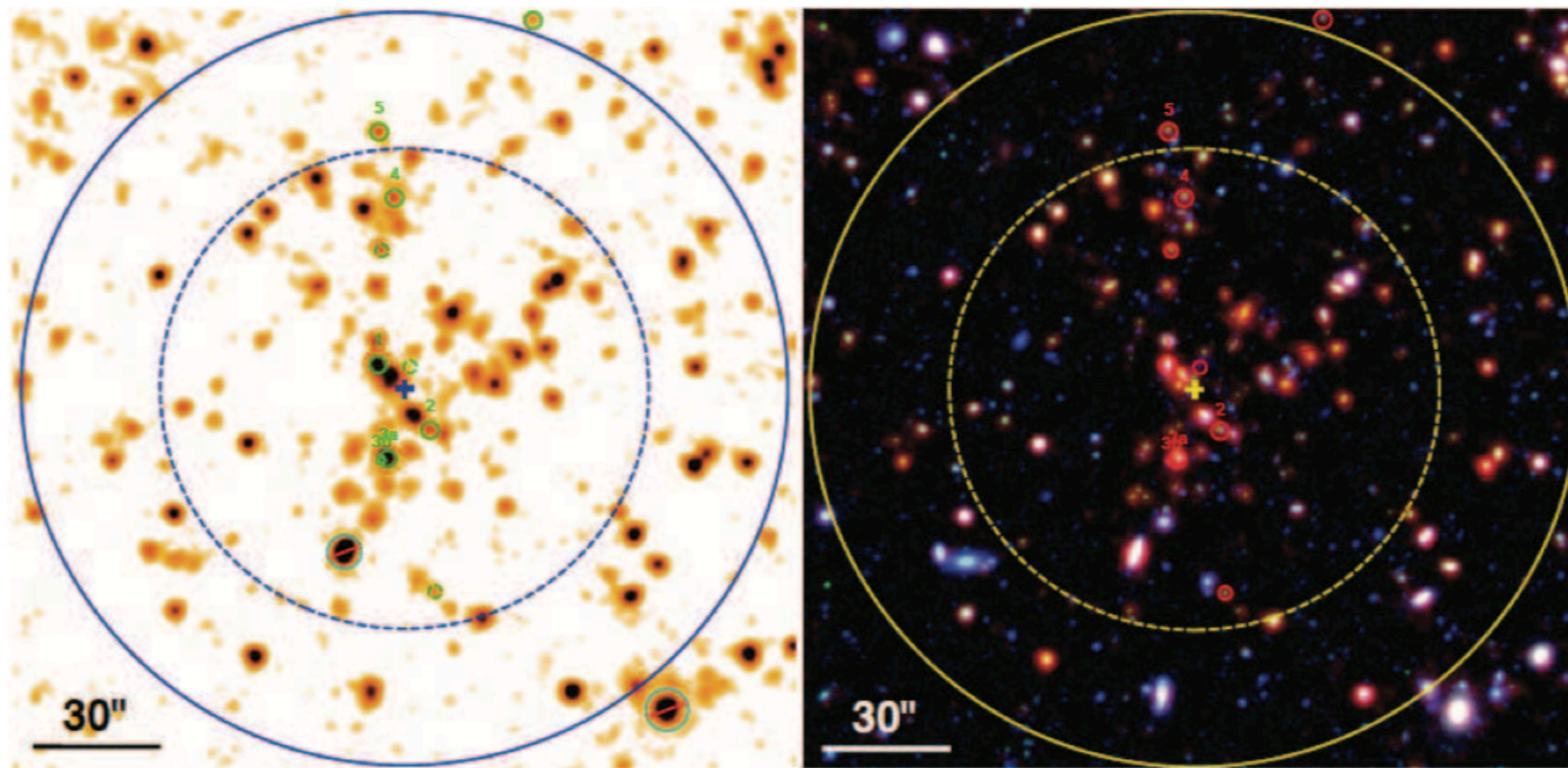
inner part. Virial radius  
1.5Mpch



Fassbender et al.2018: The highest mass cluster with an observed high star formation activity is the recently discovered system SPT-CL J2040-4451 at  $z = 1.48$  with a mass of  $M_{200} \approx 6 \times 10^{14} M_{\odot}$  (Bayliss et al. 2013).

XMMU J2235.3-2557 at  $z = 1.39$  with  $M_{200} \approx 7 \times 10^{14} M_{\odot}$  (Rosati et al. 2009) is the highest redshift cluster with a fully quenched core region within 200kpc (Strazzullo et al. 2010; Bauer et al. 2011; Grützbauch et al. 2012).

### X-ray luminous galaxy cluster XDCP J0044.0-2033 at $z = 1.58$



From the original total mass estimate of  $M_{200} \approx 3 \times 10^{14} M_{\odot}$  we can approximate the characteristic cluster radii to be  $R_{200} \approx 760$  kpc  $\approx 90''$  and  $R_{500} \approx 490$  kpc  $\approx 58''$ .

**Fig. 6.** *Left panel:* Spitzer/IRAC 4.5 $\mu$ m view of the cluster volume (3'  $\times$  3'). The cluster center (central cross),  $R_{500}$  (dashed blue circle), and  $R_{200}$  (solid blue circle) are indicated, small circles mark spectroscopic members as in Fig. 2. The crossed-out cyan objects were removed from the analysis. *Right panel:* color composite with the same FoV by adding the V-band (blue) and the combined J+Ks image (green) to the Spitzer 4.5 $\mu$ m data (red).

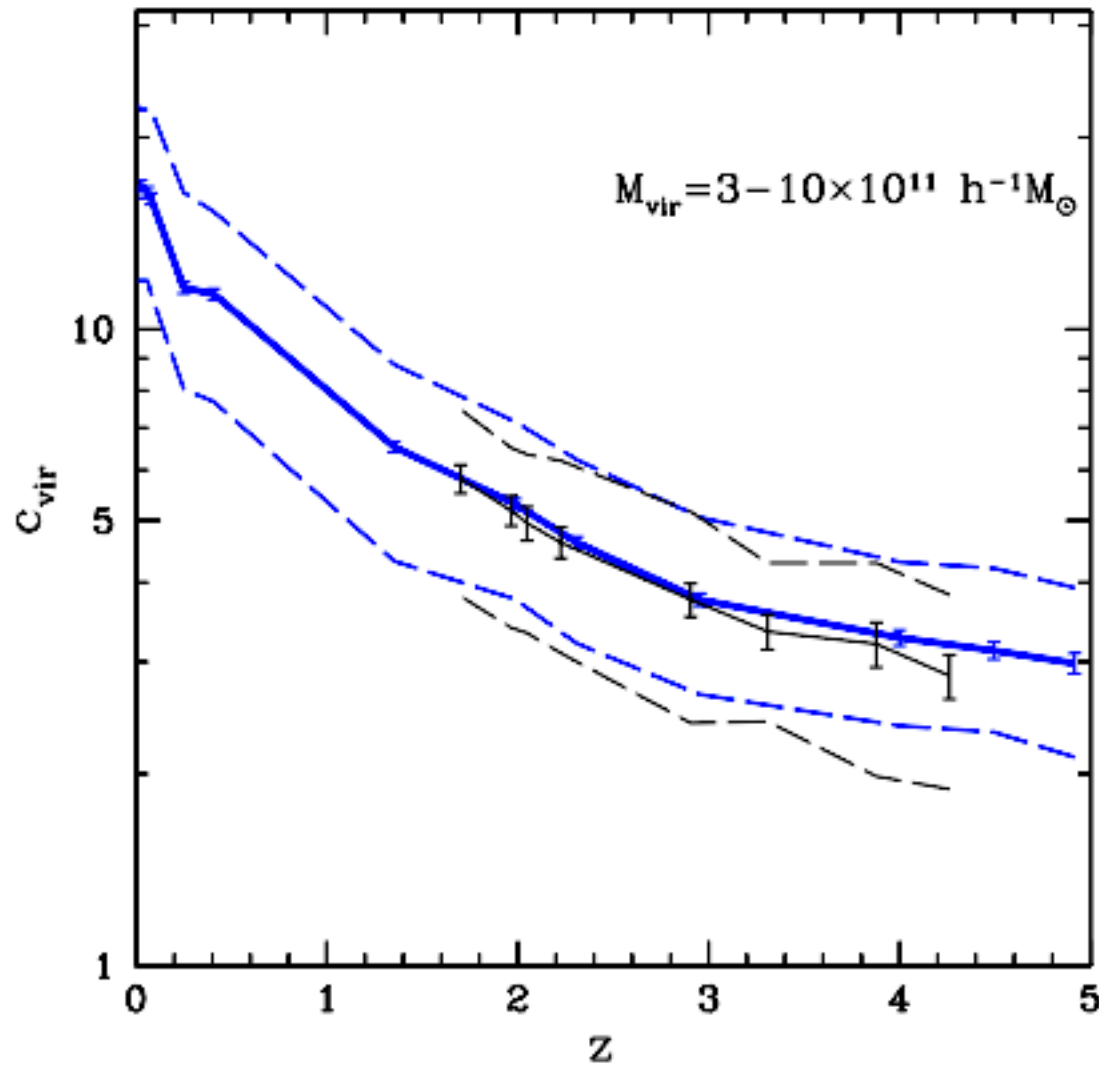


**Figure 3.** Convergence test for  $c_{\text{vir}}$  evolution and scatter. Shown is a comparison of  $M_{\text{vir}} = 3 - 10 \times 10^{11} h^{-1} M_{\odot}$  haloes simulated using our main simulation (thick lines) and a second simulation with 8 times the mass resolution (thin lines). The solid lines and errors reflect the median and Poisson uncertainty respectively. The dashed lines reflect the estimated intrinsic scatter. There is no evidence for significant deviations in either the measured median or scatter as the mass resolution is increased.

- Main trend with redshift for a fixed halo mass

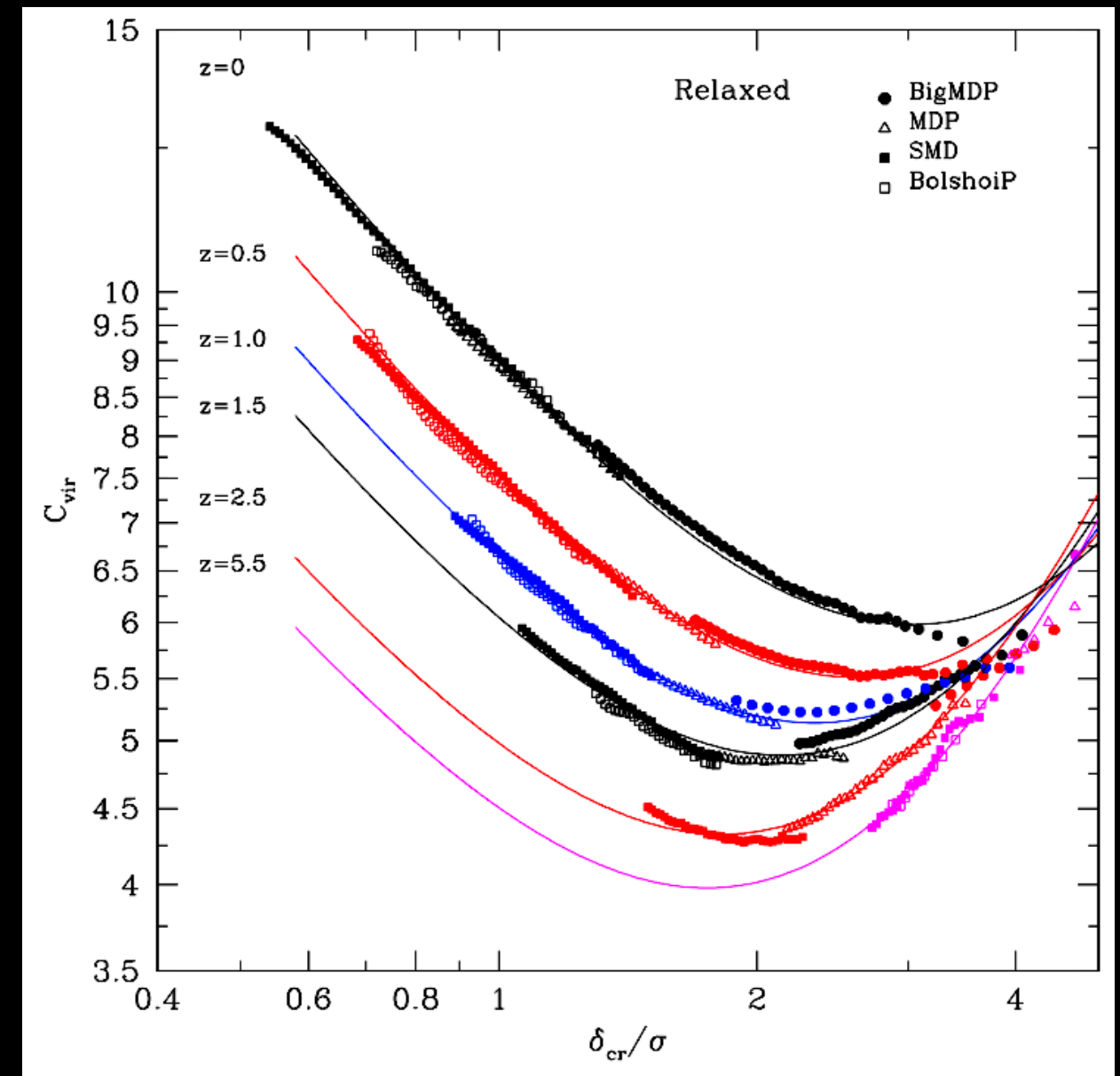
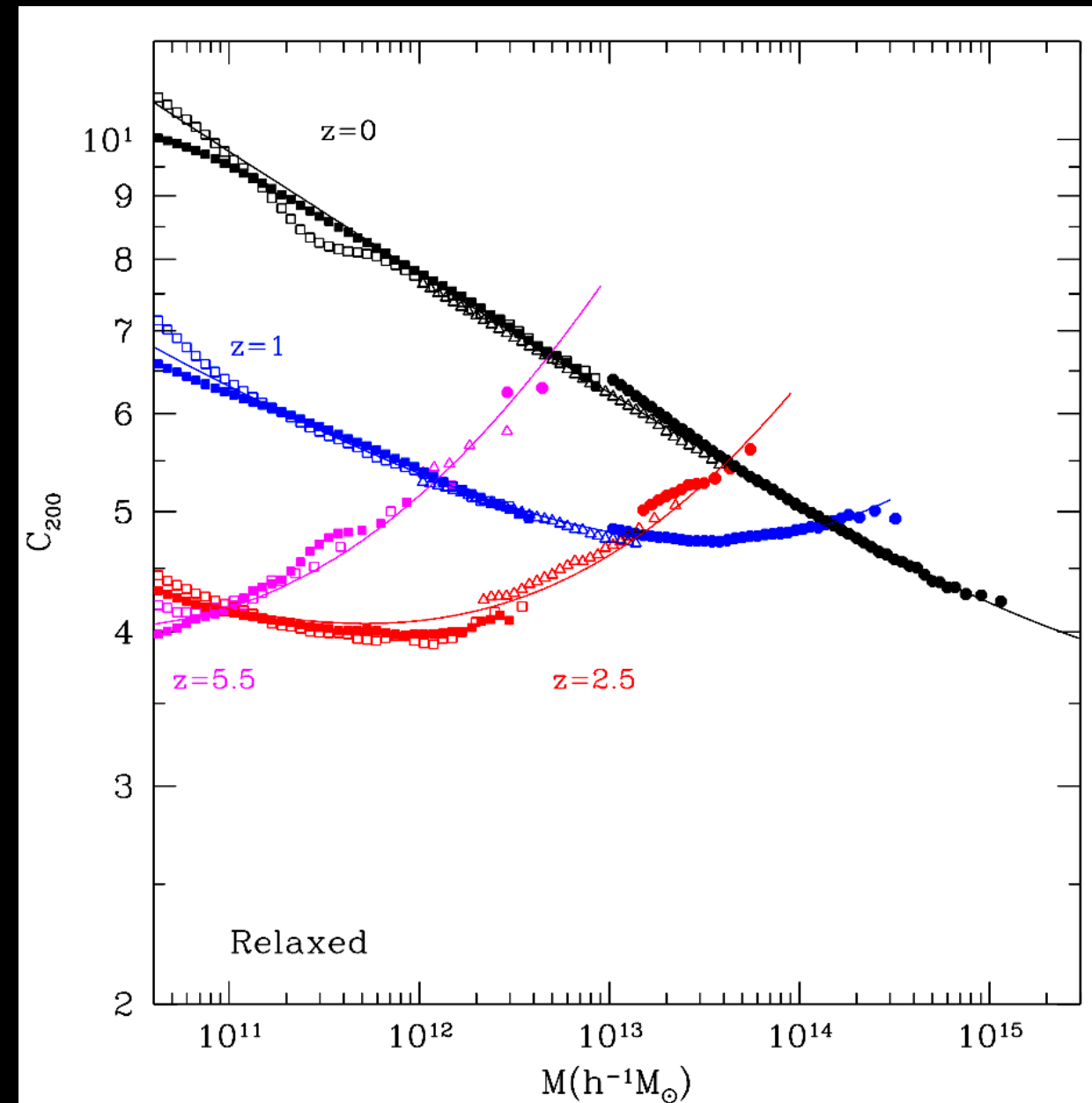
$$c_{\text{vir}}(a) \propto a.$$

$$C \equiv \frac{r_{\text{vir}}}{r_s},$$

$$r_{\text{vir}}(M_{\text{vir}}) = 443 h^{-1} \text{ kpc} \left( \frac{M_{\text{vir}} / 10^{11} h^{-1} M_{\odot}}{\Omega_0 \delta_{\text{th}}} \right)^{1/3}$$

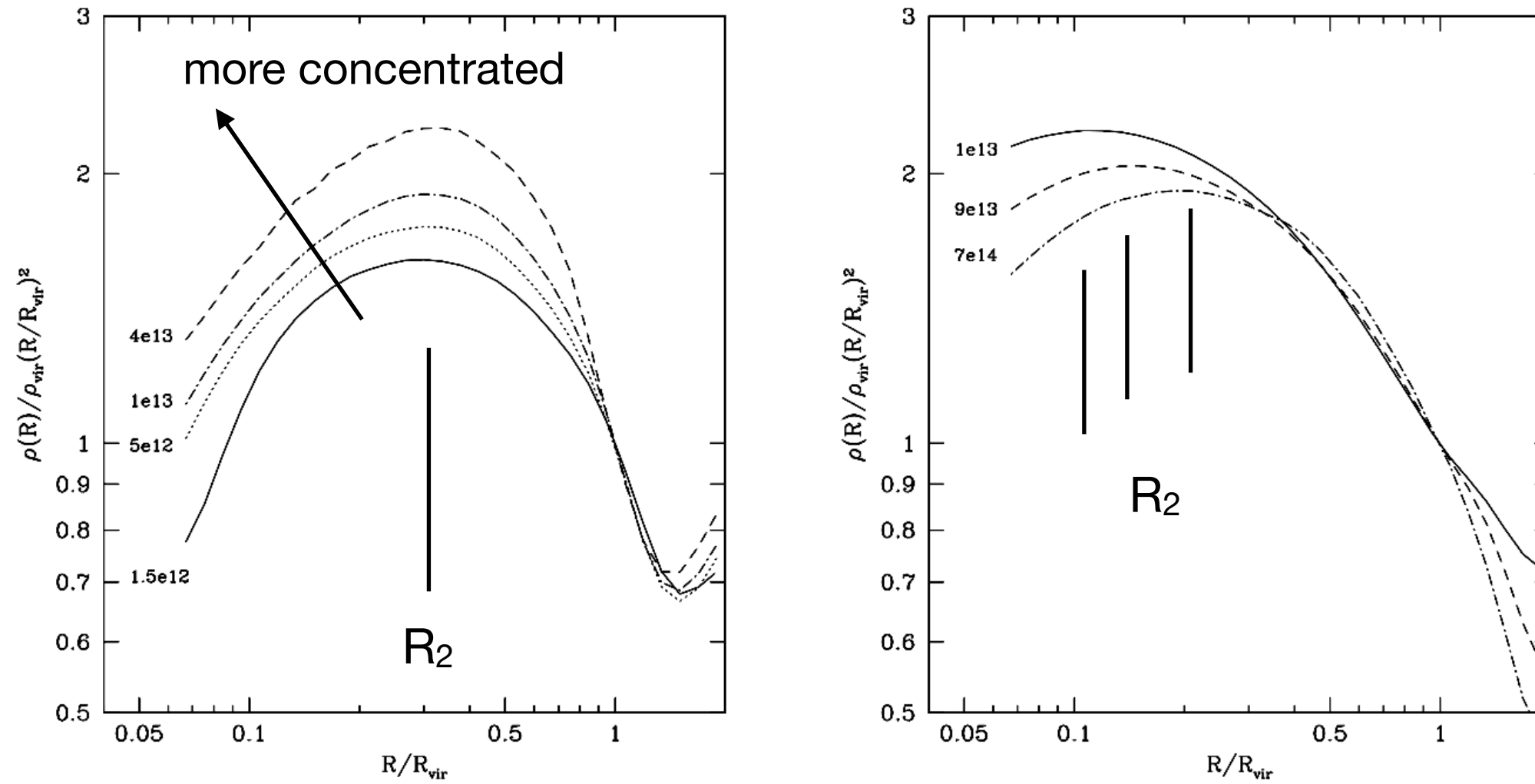
$$M_{\text{vir}} \equiv \frac{4\pi}{3} \rho_{\text{cr}} \Omega_0 \delta_{\text{th}} r_{\text{vir}}^3.$$

# Halo Concentration: need to know in order to get density profile

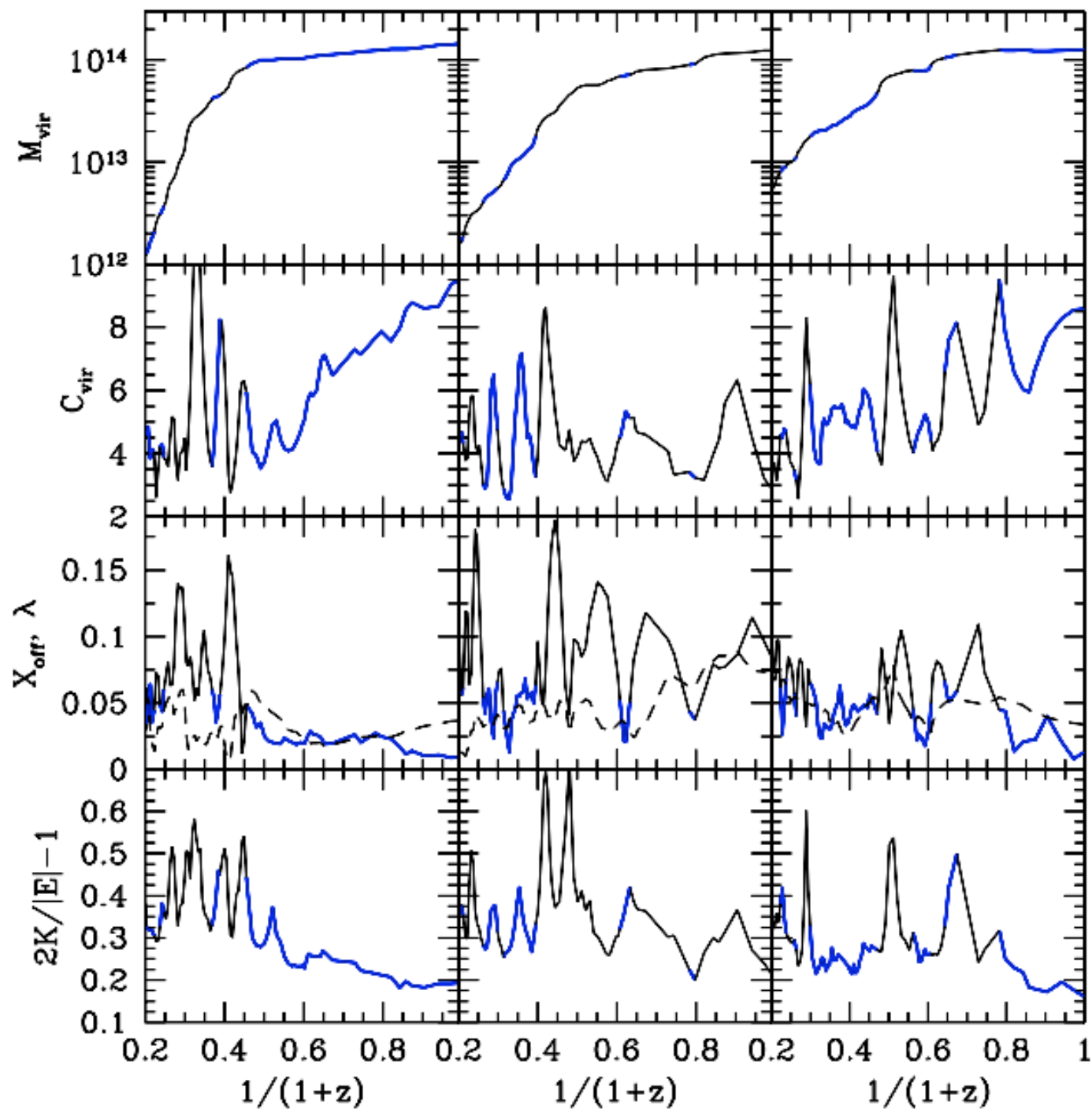


Klypin et al 2014: Gadget + ARTMultiDark suite of sims: 60G particles

## Meaning of 'concentration' depends how it is defined.



Median density profiles of relaxed halos at different redshifts and masses in N-body simulations. Profiles are normalized to have the same density at the virial radius. The left panel is for halos at  $z = 3$ : halos with larger mass are clearly more concentrated than halos with smaller masses. Similar to Einasto profiles in Figure 7, value of  $r_{-2}$  radius almost does not change with halo mass, which indicates that the increase in the concentration is mostly due to the increase in shape parameter  $\alpha$ . The right panel shows profiles of halos at  $z = 0$ . Note that the trend with mass is different: more massive halos are less concentrated and  $r_{-2}$  radius decreases with decreasing mass.



Examples of the evolution of virial mass  $M_{\text{vir}}$ , concentration  $C_{\text{vir}}$ , spin parameter  $\lambda$  (dashed curves in the second from the bottom panels), offset parameter  $X_{\text{off}}$ , and virial ratio  $2K/|E| - 1$  for 6 cluster-size halos taken from the BolshoiP simulation. Halos were selected to have  $M_{\text{vir}} \approx 10^{14} h^{-1} M_{\odot}$  and be relaxed at  $z = 0$ . Thick solid (blue) parts of the curves indicate that halos are considered to be relaxed. Large variations in halo concentration are seen at high redshifts when the halo mass increases very quickly. Once the mass accretion slows down at low redshifts, halo concentration shows the tendency to increase. Major merger events, in the right panels, seen as large jumps in mass are followed by temporary increase in halo concentration. Most of these major-merger spikes in concentration are identified as happening in non-relaxed halos.

## Effects of baryons: adiabatic contraction

---

**assumptions:** circular particle orbits, and conservation of the angular momentum:  $M(r)r = \text{const}$ , where  $M(r)$  is the total mass enclosed within radius  $r$ . With these assumptions, the final DM distribution is calculated given the initial mass profiles  $M_{\text{dm}}(r)$ ,  $M_b(r)$  and final baryon profile  $M_b(r_f)$ :

$$[M_{\text{dm}}(r) + M_b(r)]r = [M_{\text{dm}}(r) + M_b(r_f)]r_f.$$

the average radius along the orbit,  $\bar{r}$ ,

adiabatic contraction model based on conservation of the product of the current radius and the mass enclosed within the orbit-averaged radius:

The orbit-averaged radius is

$$\bar{r} = \frac{2}{T_r} \int_{r_p}^{r_a} r \frac{dr}{v_r},$$

$$M(\bar{r})r = \text{const.} \quad (6)$$

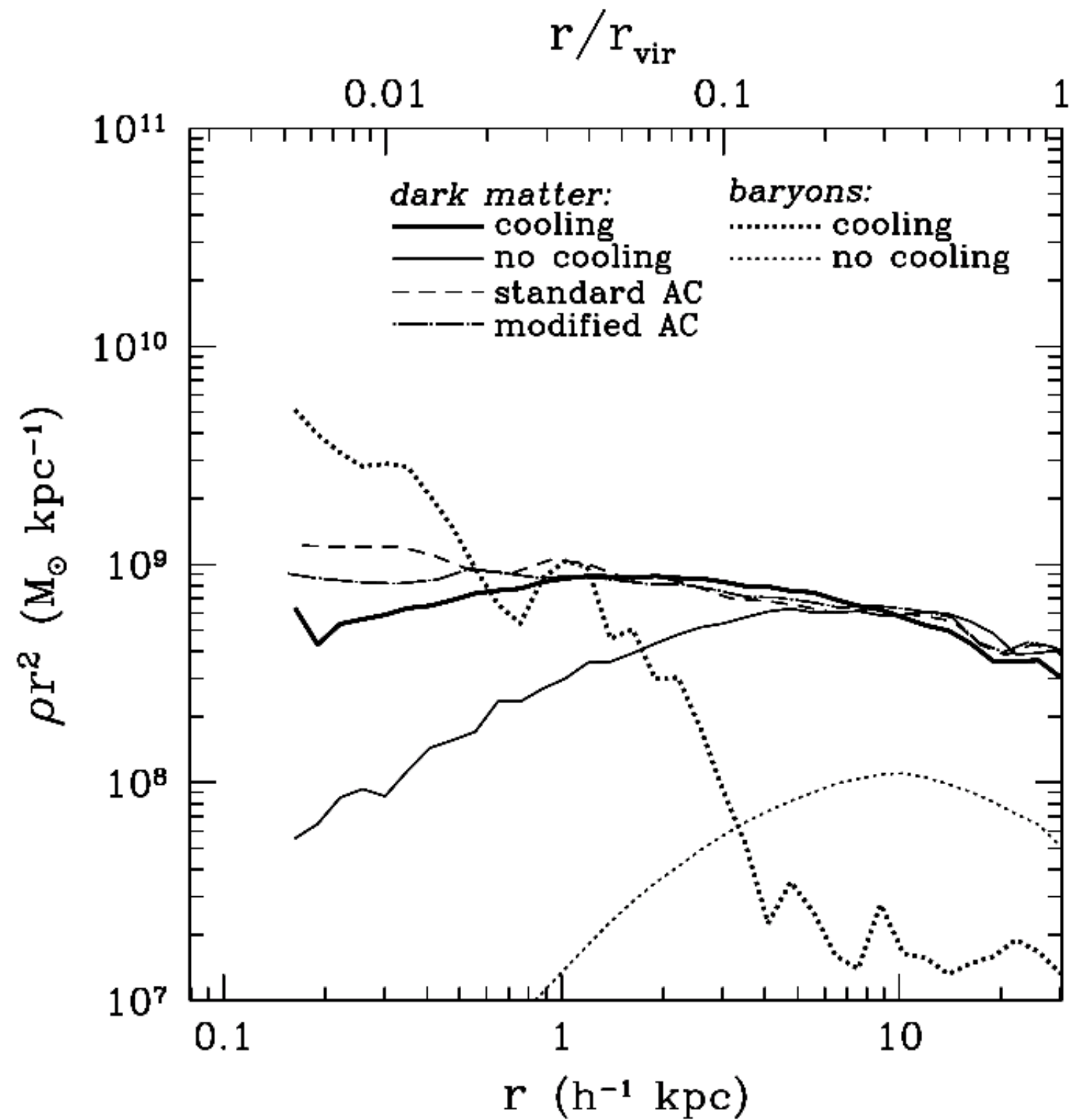
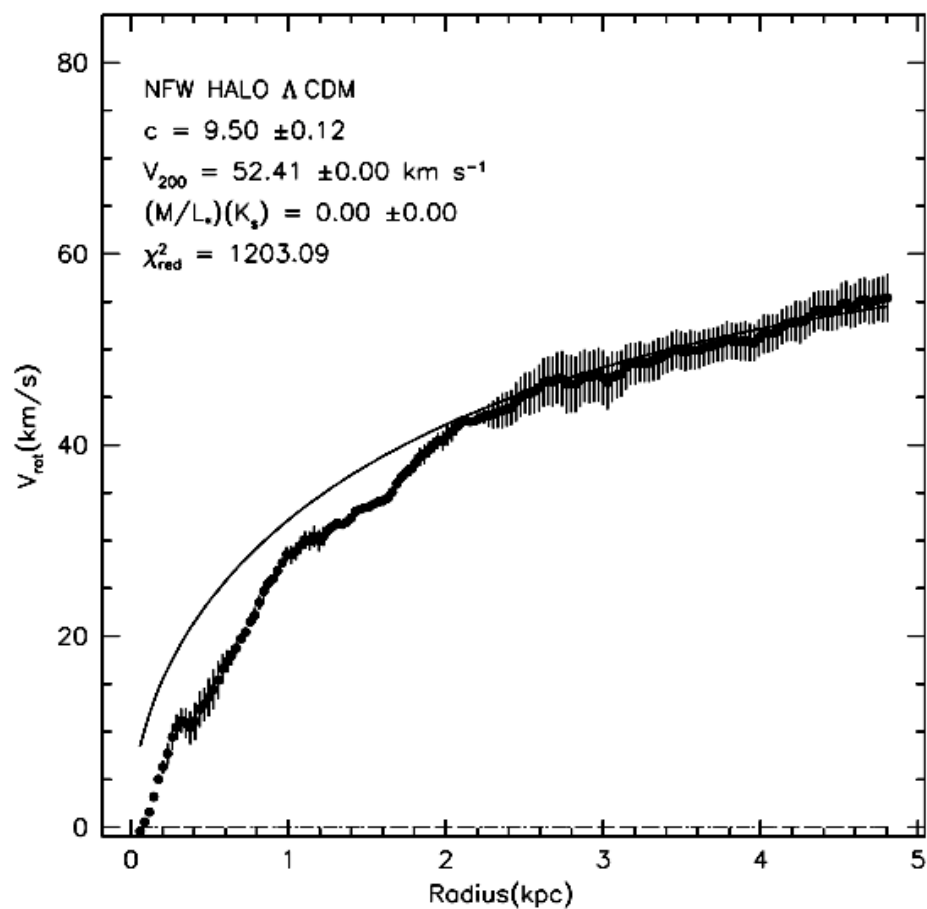
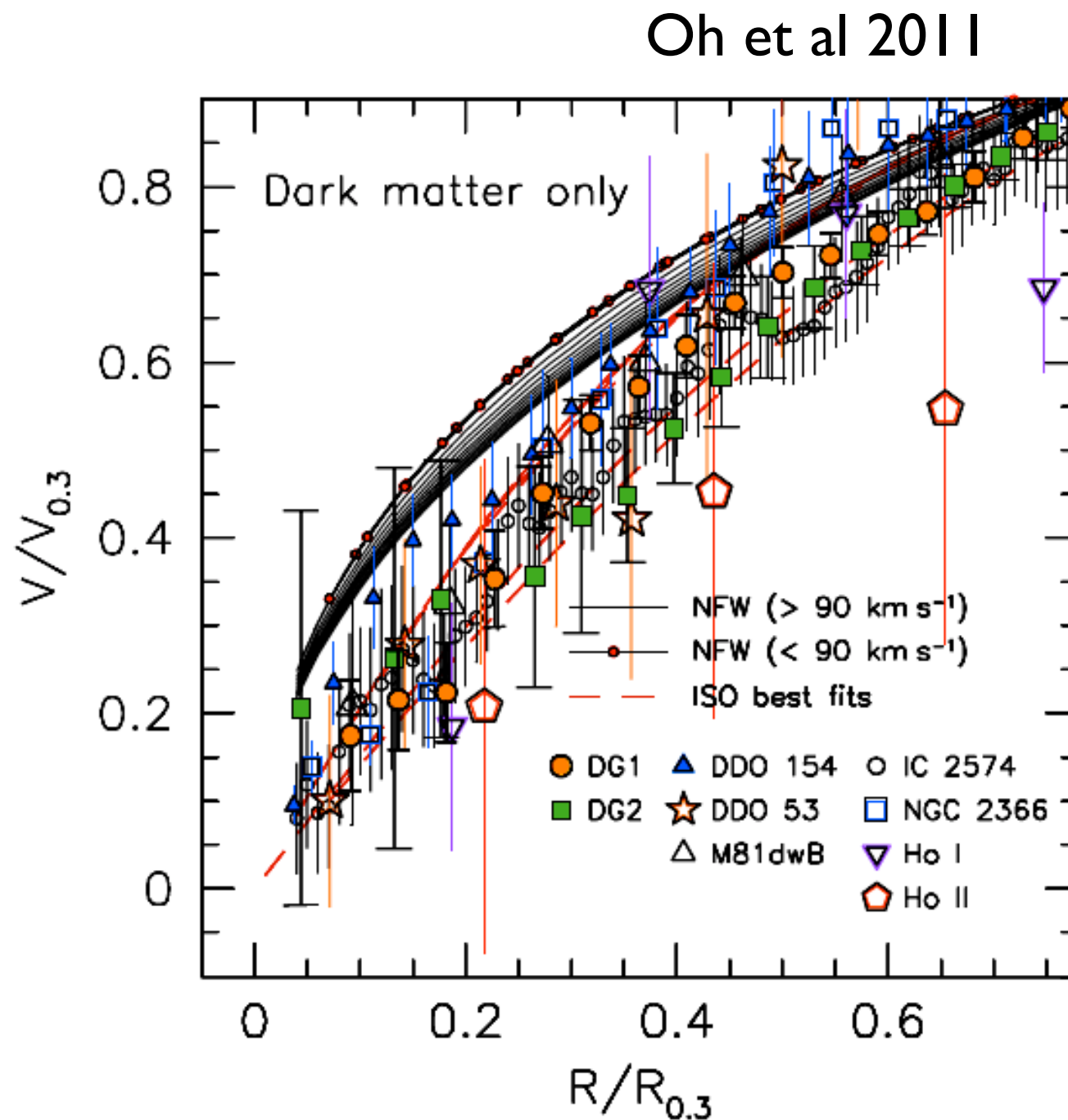


FIG. 3.—Density profile in the galaxy formation run at  $z = 4$  as a function of physical radius. Lines types are as in Fig. 1. [See the electronic edition of

# Density Profiles: Mass at $\sim 1$ kpc radius. Core-cusp problem



NGC 6822, de Blok et al 2007



**N**umerous episodes of baryon infall followed by a strong burst of star formation, which expels the baryons. At the beginning of each episode the baryons dominate the gravitational potential. The DM contracts to respond to the changed potential. A sudden onset of star formation drives the baryons out. The DM also moves out because of the shallower potential. Each episode produces a relatively small effect on the DM, but a large number of them results in a significant decline of the DM density. Indeed, cosmological simulations that implement this process show a strong decline of the DM density. Whether the process happens in reality is still unclear.

**S**imulations with the cycles of infall-burst-expansion show flattening of the DM cusp may occur. If this happened to our Galaxy, then the DM density within the central  $\sim 500$  pc may become constant. This would reduce the annihilation signal by orders of magnitude. We note that this mechanism would wipe out the DM cusp also in centers of dwarf galaxies.

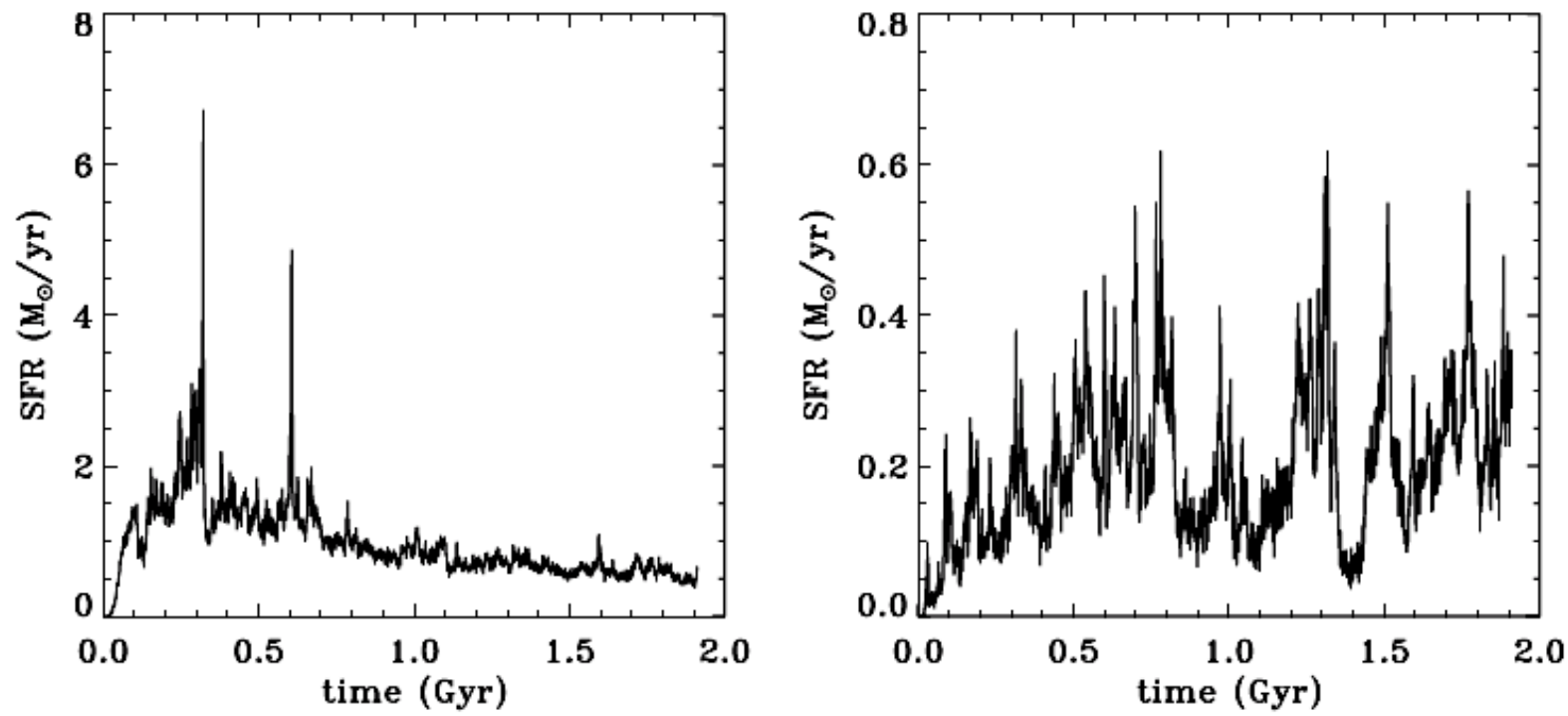


Figure 3. Star formation history in the runs without (left-hand plot) and with (right-hand plot) feedback.

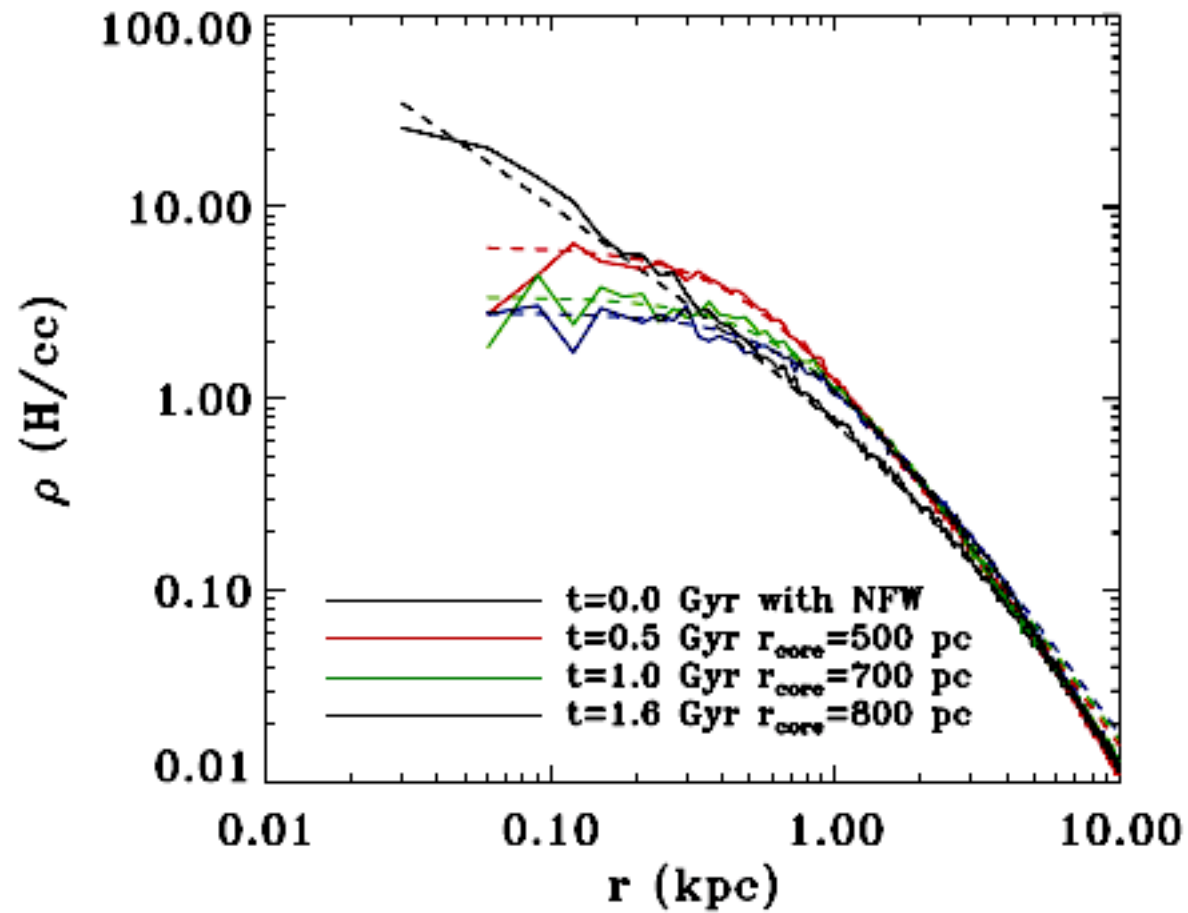
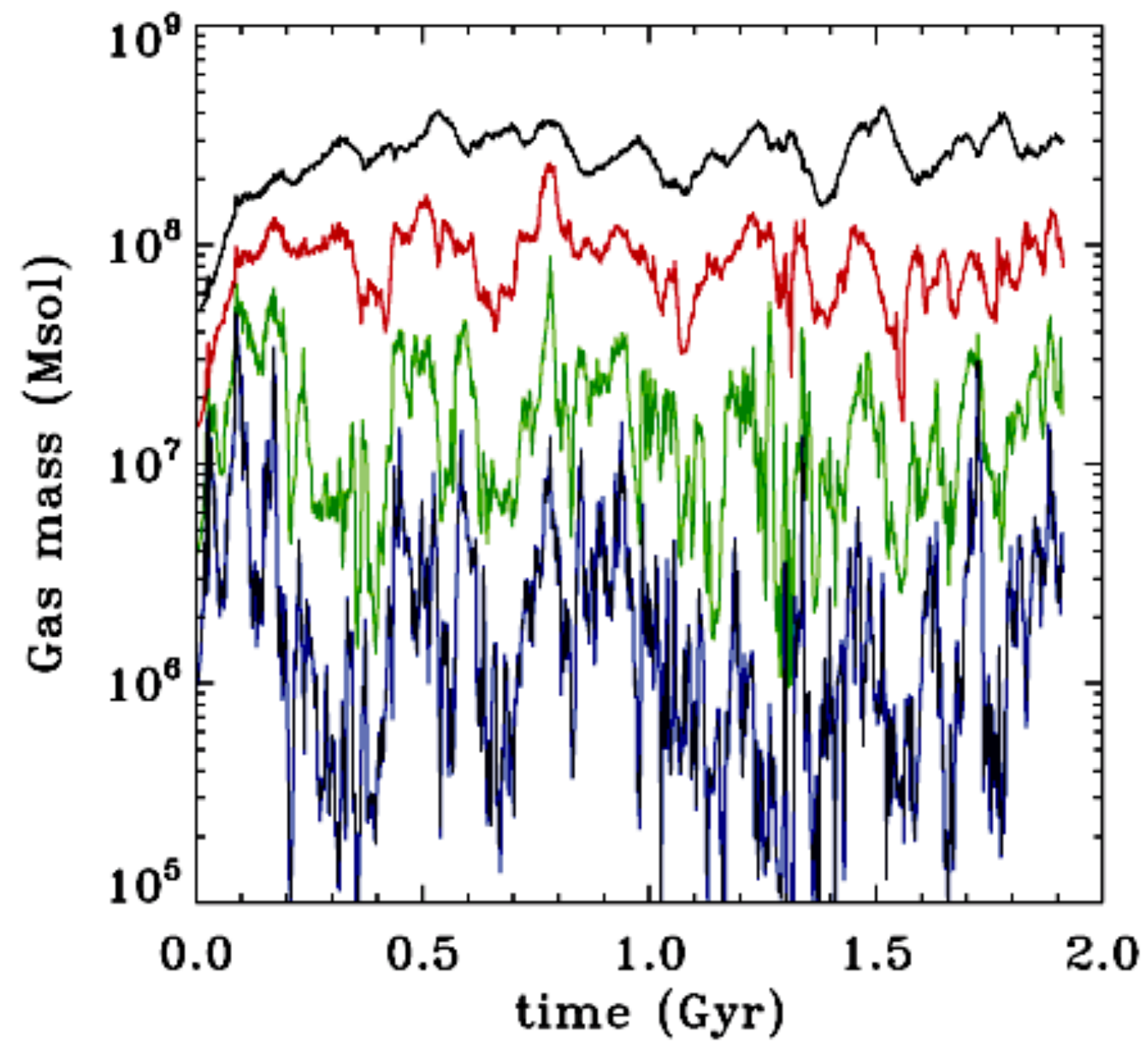


Figure 5. Evolution of the dark matter density profile over the 2Gyr of evolution for the control run with cooling, star formation and stellar feedback. We see the formation of a large core. We also show for comparison the analytical fit (dashed line) based on a pseudo-isothermal profile.



**Figure 7.** Time evolution of the total enclosed gas mass within spheres of radii 200 (blue), 400 (green), 800 (red) and 1600 (black) pc for the simulation with feedback.